Mantle structural geology from seismic anisotropy

Paul R Silver, David R Mainprice, Walid Ben Ismaïl, Andrea Tommasi, Guilhem Barruol

Mantle Petrology: Field Observations and high Pressure experimentations: a Tribute to Francis R. (Joe) Boyd
© The Geochemical Society, Special Publication N° 6, 1999
Editors: Yingwei Fei, Constance M. Bertka, and Bjorn O. Mysen

Mantle structural geology from seismic anisotropy

PAUL SILVER[1], DAVID MAINPRICE[2], WALID BEN ISMAÏL[2], ANDRÉA TOMMASI[2], and GUILHEM BARRUOL[2]

[1]Department of Terrestrial Magnetism, 5241 Broad Branch Road, N.W., Washington, DC 20015, U.S.A.
[2]Laboratoire de Tectonophysique, ISTEEM, CNRS UMR 5558, Université Montpellier II, 34095 Montpellier cedex 05, France.

Abstract--Seismic anisotropy is a ubiquitous feature of the subcontinental mantle. This can be inferred both from direct seismic observations of shear wave splitting from teleseismic shear waves, as well as the petrofabric analyses of mantle nodules from kimberlite pipes. The anisotropy is principally due to the strain-induced lattice preferred orientation (LPO) of olivine. The combined use of these mantle samples, deformation experiments on olivine, and numerical modeling of LPO, provides a critical framework for making inferences about mantle deformation from observed seismic anisotropy. In most cases there is a close correspondence between mantle deformation derived from seismic observations of anisotropy, and crustal deformation, from the Archean to the present. This implies that the mantle plays a major, if not dominant role in continental deformation. No clear evidence is found for a continental asthenospheric decoupling zone, suggesting that continents are probably coupled to general mantle circulation.

INTRODUCTION

The mantle nodules that are brought to the surface by kimberlitic eruptions form the foundation for inferring the geological properties of the subcontinental mantle. These rocks provide a unique means of constraining the composition, petrology, temperature, pressure, age, and physical properties of the subcontinental mantle. JOE BOYD has been the leader in recognizing and exploiting the valuable information that these rocks contain. More recently, these same rocks have also been used to constrain the degree and style of deformation in the subcontinental mantle, through a comparison of the petrofabrics in these rocks and the observations of seismic anisotropy that are produced by this fabric. There has been a rapidly growing interest in seismic anisotropy as a way of constraining the deformation of the continental upper mantle. There are two basic problems that can be addressed with this approach: the deformation of the mantle portion of continental plates, and the mantle flow field beneath these plates. The first problem represents a natural extension of structural geology into the mantle and down to the base of the plate. The second problem addresses the nature of the mantle flow field just below the plates, down to the transition zone. A major stimulus for the recent focus on the study of mantle deformation is the rapid increase in the number of observations related to anisotropy. This has come from the establishment, over the last decade, of a global network of broadband seismographs, and perhaps more importantly, from the deployment of portable instruments, which allow for the collection of anisotropy data in particular regions of geologic interest.

Shear-wave splitting observations are the most unambiguous manifestation of anisotropy available to seismologists. They are also very simple and robust measurements that are now made routinely. Their utility in constraining subcontinental mantle deformation is analogous to the use of isotropic travel times as a means of studying variations in mantle temperature and composition. As integral functions of the anisotropy along the path of the shear wave, they provide valuable information about flow and deformation in the upper mantle. While measuring the splitting parameters is a reasonably straightforward seismological task, working out the relationship between anisotropy and mantle deformation is somewhat less so, as it involves knowledge from a variety of disciplines. The basis for this relationship is the development of lattice preferred orientation (LPO) in upper mantle rocks containing the anisotropic mineral olivine. One is interested in using anisotropy to map mantle deformation as a way of testing dynamic models of mountain building or mantle flow characteristics associated with the past and present motion of plates. To go from the deformation generated by a particular tectonic process to the prediction of splitting parameters, one needs to: i) presume the deformation field that is developed by that tectonic process (*e.g.*, mountain building), ii) determine the resulting LPO of upper mantle aggregates from finite strain and calculate the aggregate elastic constants, and iii) calculate the seismological manifestation of anisotropy for this medium, incorporating the appropriate geometry.

With these relationships in place, it is possible to predict the characteristics of seismic anisotropy for a particular tectonic process. (iii) is the realm of seismology, and within it are the various seismological manifestations of a specified anisotropic medium. (ii) is the domain of petrophysics/mineral physics and rock mechanics, and involves such issues as the single-crystal

properties of upper mantle minerals, the rheological behavior of mineral aggregates under finite strain (including recrystallization), and the quantification of strain indicators, such as those based on microtexture. One of the most important sources of information concerning the petrophysical constraints is the suite of kimberlitic mantle nodules; as we will see, these mantle samples play a crucial role in the interpretation of seismic anisotropy. The linking together of seismic anisotropy and LPO constitutes the forward problem of determining the anisotropic properties of upper mantle deformation. We next seek to ascribe a physical process to the observed anisotropy, in which case it is necessary to predict the deformation field that the process creates, and this corresponds to (i) above. The generation of this deformation or flow field has been traditionally the domain of mantle dynamics, applied both to mantle convection and plate (usually continental) deformation. There has recently been renewed interest among geodynamicists in making anisotropic predictions of mantle flow models as an important way of testing such models (BUTTLES and OLSON, 1998; CHASTEL *et al*. 1993; BLACKMAN *et al*., 1996; BLACKMAN and KENDALL,1997; FOUCH *et al*., 1999; KINCAID and SILVER, 1996; DAVIS *et al*., 1997; TOMMASI *et al*., 1996; TOMMASI, 1998). This is a healthy trend that will make the maximum use of the constraints that anisotropy provides. We will consider later two simple physical processes that have straightforward anisotropic characteristics.

CONTINENTAL ANISOTROPY: SUMMARY OF SHEAR WAVE SPLITTING OBSERVATIONS.

In an isotropic, homogeneous medium there are two types of body waves, a P and an S wave; in an anisotropic medium, there are three, a quasi-P wave and two quasi-shear waves. For weak anisotropy (the case encountered in the Earth), the P and S wave displacement directions are still, in most cases, nearly parallel and perpendicular, respectively, to the propagation direction, as for an isotropic medium. Shear-wave splitting refers to the fact that the two shear waves have polarizations that are orthogonal to each other and propagate at different velocities. For a homogeneous medium, the velocities (V) and displacement directions of the three waves are given by the eigenvalues and eigenvectors of the second order tensor velocity matrix T_{il} defined by the Christoffel equation:

$$| T_{il} - \rho V^2 \delta_{il} | = 0, \quad T_{il} = C_{ijkl} n_j n_k \qquad (1)$$

where δ_{il} is the Kronecker delta, C_{ijkl} is the elasticity tensor for the medium, **n** is a unit vector that defines the propagation direction, and ρ is density. The two splitting parameters obtained from seismic data are the polarization direction of the fast shear wave ϕ and the delay time δt between the arrival time of the fast and slow shear waves (Fig. 1). From (1) it is found that δt is proportional to path length L according to the approximate expression for small anisotropy: $\delta t = L\delta V_s / \langle V_s \rangle$ where $\langle V_s \rangle$ is the isotropically averaged shear velocity and δV_s is the dimensionless intrinsic anisotropy, which is a function of **n** (SILVER and CHAN, 1991). As we will see, ϕ is related to the orientation of the mantle strain field. Splitting in teleseismic shear waves such as SKS and S (See Fig. 1) is particularly useful in assessing the mantle's role in geological processes, because of the excellent lateral resolution (about 50km) for the periods typically used in splitting analyses. Thus small geologic domains, and the boundaries between domains can be carefully sampled. The vertical resolution is not good, since the anisotropy could, in principle, reside anywhere between the core-mantle boundary (CMB) and the surface in the case of SKS (Fig. 1). As shown below, however, the dominant source of anisotropy in shear-wave splitting is most probably in the upper mantle beneath the recording station.

There are presently over 400 observations of splitting in teleseismic shear waves (SAVAGE, 1999). These represent a combination of permanent stations as well as a large number of portable experiments where splitting parameters have been obtained in areas of specific geologic interest. There have been two recent reviews (SILVER, 1996; SAVAGE, 1999) that will provide the reader with a general overview of the shear wave splitting data set. The highlights are given here. There are splitting observations from essentially all continents, although the two with the most observations are North America and Eurasia. The mean value of splitting delay times is about 1 s (SILVER, 1996). Assuming about 4% intrinsic anisotropy, this corresponds to about a 100 km thick layer of anisotropic mantle. The range is from barely detectable (less than 0.5 s) to 2.4 s. There are only a few measurements above δt=2 s. There are also about 10% of the data set where splitting was not detected. This means that anisotropy is a near-ubiquitous feature of the subcontinental region.

The dominant contribution to the splitting is from the upper mantle. There is a crustal contribution, but it is small A variety of studies have focused on crustal splitting (see SILVER, 1996; SAVAGE, 1999, and references therein). Crustal anisotropy values are obtained from: 1) the recording of crustal earthquakes just below the station, 2) shear waves from events occurring in a subducting slab that pass only through the crust of the overlying plate, and 3) the analysis of splitting in P to S conversions at the Moho, which isolate the crustal component of splitting. Each of these methods point to a range in splitting parameters of 0.1 to 0.3s, with occasional values up to 0.5 s, and

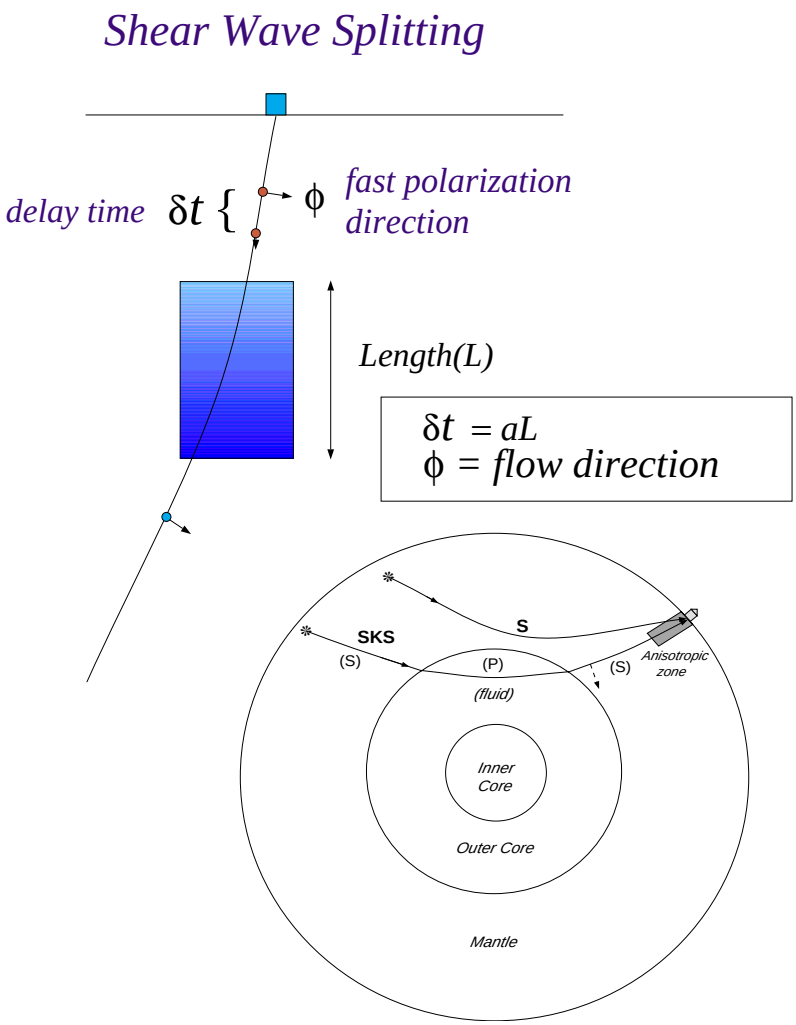

FIG. 1. (a) Schematic of shear wave splitting. A shear wave entering an anisotropic medium is split into two shear waves with different velocities and orthogonal polarizations. The two splitting parameters that can be obtained from data are the fast polarization direction ϕ and delay time δt. between the two arrivals. Teleseismic shear waves SKS and S are most commonly used.

an average of about 0.2 s. The delay time does not appear to be a function of crustal thickness. For example, crustal delay times on the Tibetan Plateau (MCNAMARA *et al*., 1994), with an average crustal thickness of 70 km also fall within the normal range of 0.1 to 0.3s. This suggests that the crustal anisotropy is dominated by cracks in the top 10-15 km of the crust.

The long path through the transition zone and lower mantle could also contribute to the splitting recorded at continental stations. Yet, this contribution appears to be small as well, for the following reasons: (i) Significant variations in SKS splitting parameters are frequently observed for stations that are separated by 50-100 km (*e.g.*, SILVER and KANESHIMA, 1993). This requires that the regions of the mantle that the wave samples, the first Fresnel zone, are independent of each other. This generally restricts the anisotropic zones to be in the upper mantle, for stations that are separated by about one hundred kilometers. (ii) For a given station, the splitting parameters for SKS at different backazimuths, as well as direct S waves from deep focus events (where there is probably no contribution from the source-side upper mantle) are usually compatible with each other (see MCNAMARA *et al*., 1994; KANESHIMA and SILVER, 1995), although the paths through the lower mantle are very different. (iii) Using the special geometry afforded by locally recorded subduction zone events, it is

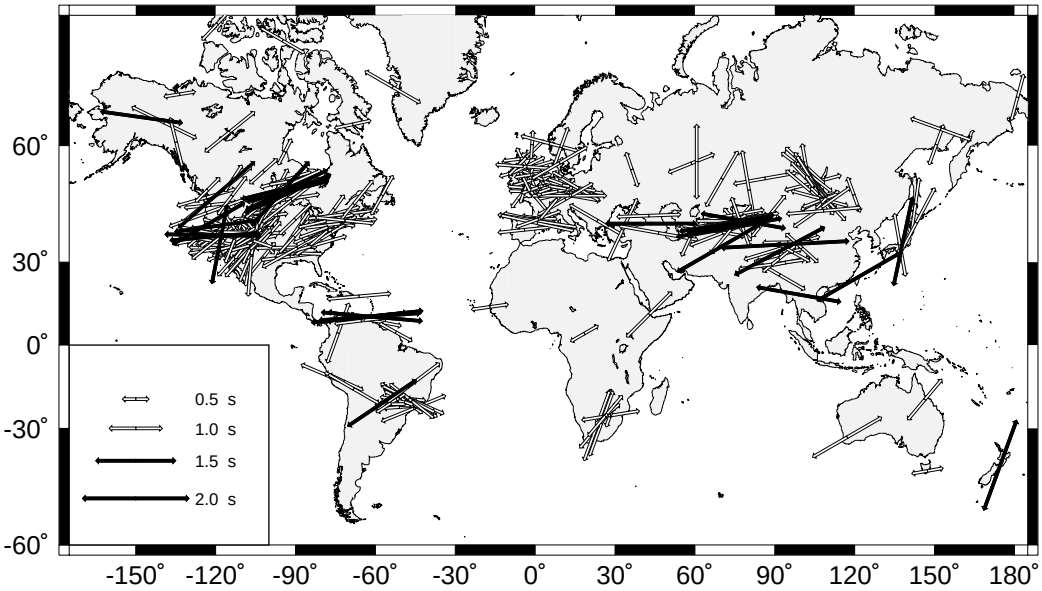

FIG. 1. (b) Map of world with data set of splitting parameters from SILVER (1996). Orientation of line gives fast polarization direction and length of line is proportional to delay time according to the legend. Black symbols correspond to delay times in excess of 1.5 s. Note that most of the large delay times are found either in present-day transpressional zones (Alpine-Himalayan chain, Australian/Pacific plate boundary at New Zealand, South American/Caribbean plate boundary in Venezuela, Alaskan Cordillera) or Archean transpressional zones, such as the western Superior province of the Canadian Shield. Most of the measurements are concentrated in the Northern Hemisphere, in North America and Eurasia.

possible to compare directly the splitting parameters of upward propagating S waves from intermediate and deep focus events that sample exclusively the upper mantle, with those for SKS and ScS at close distance that sample the lower mantle (once for SKS, twice for ScS) as well as nearly the same upper mantle path (KANESHIMA and SILVER, 1995; MEADE *et al*., 1995; SAVAGE, 1999). No significant difference in delay time is observed, restricting the lower mantle contribution to under about 0.2 s. There have recently been observations of splitting from S waves traveling nearly horizontally near the core-mantle boundary (*e.g.*, see KENDALL and SILVER, 1996; 1998), although this appears to be dominantly transverse isotropy with a vertical symmetry axis, which would not affect the SKS observations because SKS is radially polarized as it leaves the core-mantle boundary.

As noted in Fig. 1b, one of the significant features of the splitting data set is that the largest delay times, corresponding to the largest anisotropic effect, are often found in regions of present day transpressional zones, such as the Alpine-Himalayan chain or ancient ones, such as the Western Superior Province of the Canadian Shield. As we will see, these zones are central to understanding the physical basis for the observed anisotropy.

INTERPRETING THE SEISMIC ANISOTROPY DATA SET: PETROPHYSICAL CONSIDERATIONS

In order to correctly interpret seismic anisotropy as a constraint on mantle deformation, it is necessary to know: (i) the minerals present and their volume fractions in the upper mantle as a function of depth, (ii) the single-crystal elastic constants of the minerals at the temperatures and pressures of the upper mantle, (iii) how the crystal orientations (LPO) evolves during plastic deformation in the flow field of the upper mantle, and (iv) the orientation of the structural frame or flow field in the mantle. (i) can be determined by direct observations on mantle nodules from the top 220 km of the upper mantle (BOYD, 1973) and ophiolite massifs for the top section of the oceanic upper mantle (NICOLAS, 1989), from experimental petrology (BOYD and ENGLAND, 1960, RINGWOOD, 1991), or from petrological models such as pyrolite and piclogite (*e.g.*, ITA and STRIXRUDE, 1992) derived from experimental studies. (ii) can be determined in a straightforward manner from laboratory measurements (see compilation by BASS, 1995). We will briefly review the situation for the upper mantle because of the large number of single crystal elastic

constant determinations since 1995. The properties of deformation in upper mantle aggregates (iii) is less well characterized, and consequently has been an active area of research over the last few years. (iv) involves the much broader issue of how the mantle deforms during orogeny. We focus on the last three issues below.

Single crystal anisotropic seismic properties.

To understand the anisotropic seismic behavior of polyphase rocks in the Earth's mantle it is instructive to first consider the properties of the component single crystals. We will emphasize the anisotropy of individual minerals rather than the magnitude of velocity. The percentage anisotropy (A) is defined here as $A=200\ (V_{max} - V_{min}) /(V_{max} + V_{min})$. For P-wave velocities A is defined by the maximum and minimum velocities found by a search of all possible propagation directions. For *S*-waves in an anisotropic medium there are two orthogonally polarized S-waves with different velocities for each propagation direction. Hence S-wave anisotropy is defined for each direction and A is defined as the maximum anisotropy for all propagation directions.

The upper mantle (down to 410 km) is composed of three anisotropic and volumetrically important phases: olivine, enstatite (orthopyroxene), and diopside (clinopyroxene). The other volumetrically important phase is garnet, which is nearly isotropic and hence not of great significance to our discussion.

Olivine. A number of accurate determinations of the elastic constants of olivine are now available which all agree that the maximum anisotropy of V_p is 25% and the maximum anisotropy of V_s is 18% at ambient conditions and for a mantle composition of about Fo90. The first order temperature derivatives have been determined between 295-1500°K (ISSAK, 1992). The first and second order pressure derivatives for olivine were first determined to 3 GPa by WEBB (1989). However, a more recent determination to 17 GPa by ABRAMSON *et al.* (1997) has shown that the second order derivative is only necessary for elastic stiffness modulus C_{55}. The first order derivatives are in good agreement between these two studies. The anisotropy of the olivine single crystal increases slightly with temperature (2%) using the data of ISSAK (1992) and decreases slightly with increasing pressure using the data of ABRAMSON *et al.* (1997). One would thus expect the single crystal anisotropy to be approximately constant along a geotherm.

Orthopyroxene. The elastic properties of orthopyroxene (Enstatite or Bronzite) with a magnesium number (Mg/Mg+Fe) near the expected upper mantle value of 0.9, has also been extensively studied. The V_p anisotropy varies between 15.1% (En80 Bronzite, FRISILLO and BARSCH, 1972) and 12.0% (En100 Enstatite, WEIDNER *et al.*, 1978) and the maximum V_s anisotropy ranges between 11.0% (En100 Enstatite, WEIDNER *et al.*, 1978) and 15.1% (En80 Bronzite, WEBB and JACKSON, 1993). Some of the variation in the elastic constants and anisotropy may be related to composition and structure in the orthopyroxenes (DUFFY and VAUGHAN, 1988). The first order temperature derivatives have been determined over a limited range between 298°-623° K (FRISILLO and BARSCH, 1972). The first and second order pressure derivatives for Enstatite have been recently determined up to 12.5 GPa by CHAI *et al.* (1997) confirming an earlier study of WEBB and JACKSON (1993) to 3 GPa that showed that first and second order pressure derivatives are needed to describe the elastic constants at mantle pressures. The anisotropy of V_p and V_s does not vary significantly with pressure using the data of CHAI *et al.* (1997) to 12.5 GPa. It does increase by about 3% when extrapolating to 1000° C using the first order temperature derivatives of FRISILLO and BARSCH (1972).

Clinopyroxene. The elastic constants of clinopyroxene (Diopside) of mantle composition have only been experimentally measured at ambient conditions (LEVIEN *et al.*, 1979; COLLINS and BROWN, 1998); both studies show that V_p anisotropy is 29% and V_s anisotropy is between 20 to 24%. There are no measured single crystal pressure derivatives. In one of the first calculations of the elastic constants of a complex silicate at high pressure, MATSUI and BUSING (1984) predicted the first order pressure derivatives of diopside from 0 to 5 GPa. The calculated elastic constants at ambient conditions are in good agreement with the experimental values and the predicted anisotropy for V_p and V_s of 35.4% and 21.0% respectively is also in reasonable agreement. The predicted bulk modulus of 105 GPa is close to the experimental value of 108 GPa given by LEVIEN *et al.* (1979). The pressure derivative of the bulk modulus 6.2 is slightly lower than the value of 7.8±0.6 given by BASS *et al.* (1981). Using the elastic constants of MATSUI and BUSING (1984), the V_p anisotropy decreases from 35.4% to 27.7% and V_s anisotropy increases from 21.0% to 25.5% with increasing pressure from ambient to 5 GPa. To allow calculations of seismic properties at mantle pressures, ESTEY and DOUGLAS (1986) have proposed using the orthopyroxene pressure derivative values of FRISILLO and BARSCH (1972) but scaled down by 20%. However, comparison of the most recent orthopyroxene pressure derivatives of CHAI *et al.* (1997) with the calculated values for clinopyroxene of MATSUI and BUSING (1984) shows that they differ by 200% for C_{11}, C_{33} and C_{44} suggesting large errors would occur in using the method proposed by ESTEY and DOUGLAS (1986). We would recommend using the values given by MATSUI and BUSING (1984)

until an experimental determination has been made. A major problem still remains as no clinopyroxene temperature derivatives are available. ESTEY and DOUGLAS (1986) proposed using the orthopyroxene temperature derivatives of FRISILLO and BARSCH (1972).

In summary, the general trend favors an anisotropy decrease with increasing pressure and increase with increasing temperature. Olivine is a good example of this behavior. The changes are limited to a few percent in most cases and the primary cause of the anisotropy change is minor crystal structural rearrangements. The effect of temperature is essentially linear in all cases for the upper mantle. To illustrate the variation of anisotropy as a function of upper mantle conditions of temperature and pressure, we have calculated the seismic properties along a mantle geotherm (Fig. 2). The minerals olivine (V_p,V_s) and enstatite (V_p) show only slight increases in anisotropy in the first 100 km, so that anisotropy is expected to be roughly constant through the upper mantle.

Experiments on LPO development in olivine in aggregates.

There are surprisingly few experimental studies of LPO development in upper mantle. Two studies stand out for their contribution to our understanding of LPO development in olivine. The axial compression and simple shear experiments on synthetic olivine polycrystals at high-temperature (1200-1300°C), high strain rates (ca. 10^{-5} s^{-1}) of NICOLAS *et al.* (1973) and ZHANG and KARATO (1995) respectively. There have recently been attempts to simulate the behavior of olivine aggregates observed in the laboratory with numerical experiments. In the discussion of these experiments, it is convenient to identify a structural coordinate system, namely a foliation plane, corresponding to the maximum flattening plane, and a lineation or stretching direction that is contained within the foliation plane. It is conventional to define three structural axes as the lineation direction, *X*, the normal to the foliation plane, *Z*, and the

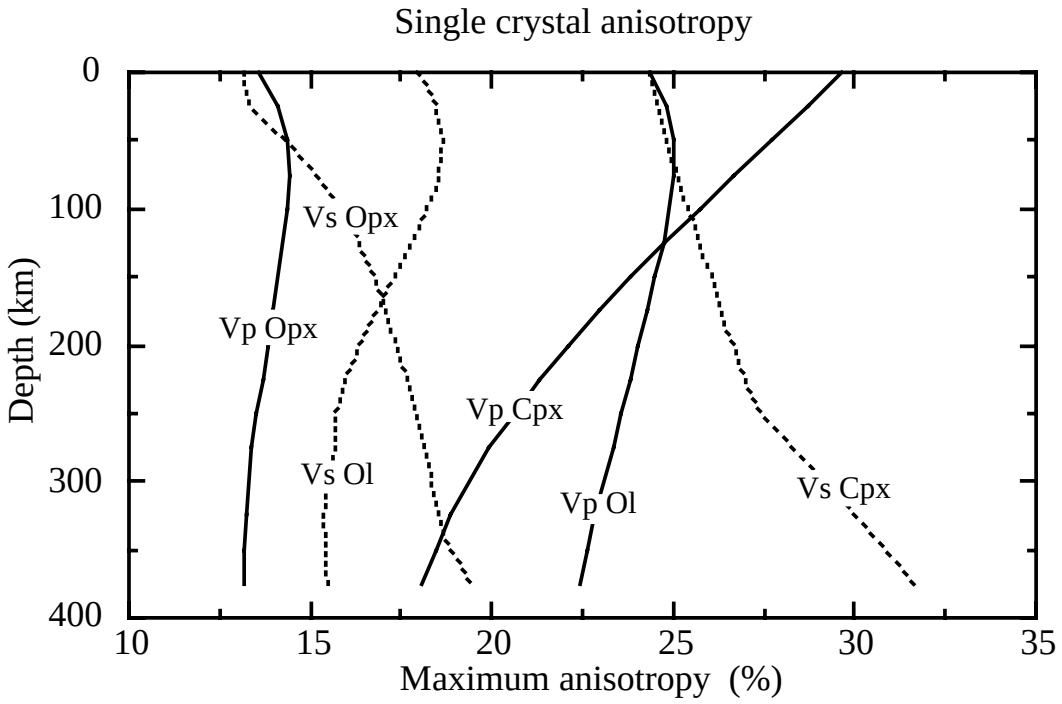

FIG. 2. The maximum seismic anisotropy of single crystals for upper mantle minerals as a function of depth along a mantle geotherm (see text for details).

direction normal to *X* in the foliation plane, *Y*. This allows the elasticity matrix inferred from the crystallographic orientation to be placed in a structural frame.

Laboratory experiments. NICOLAS *et al*. (1973) showed that in axial compression the [010] axes progressively rotate towards the compression direction, while [100] and [001] axes rotated towards the extension or flattening plane, forming a girdle normal to the shortening direction (Fig. 3). At high strains, dynamic recrystallization by nucleation of new grains within highly strained domains of the specimens was observed. At 58% axial shortening, 50% of the sample is recrystallized. The recrystallized grains and porphyroclasts display similar LPO patterns, but with a weaker LPO than the porphyroclasts (Fig. 3). This suggests that nucleation recrystallization during coaxial deformation has a dual effect on LPO intensity. Recrystallized grains display a clear misorientation relative to the parent grains, so that the LPO is weakened. On the other hand, grains in hard orientations (*e.g.*, those with [100] parallel to σ_1) suffer intense kinking (NICOLAS *et al*., 1973) and act therefore as preferential sites for recrystallization. Selective recrystallization of grains in hard orientations may help to concentrate the LPO. Fast LPO development associated with dynamic recrystallization is also observed in triaxial compression experiments ($\sigma_1>\sigma_2>\sigma_3$) under wet conditions (AVÉ-LALLEMANT, 1975). In these experiments, in which intense dynamic recrystallization occurred, strong LPO develops at lower strains than in the NICOLAS *et al*. (1973) experiments.

LPO developed in ZHANG and KARATO (1995) experiments at 1200°C display double [100] axes maxima on either side of the lineation direction (X) (Fig. 4). [010] and [001] form broad point maxima parallel to Z and Y. With increasing strain the [100] axes maximum is intermediate between the shear and lineation directions. In contrast, samples deformed

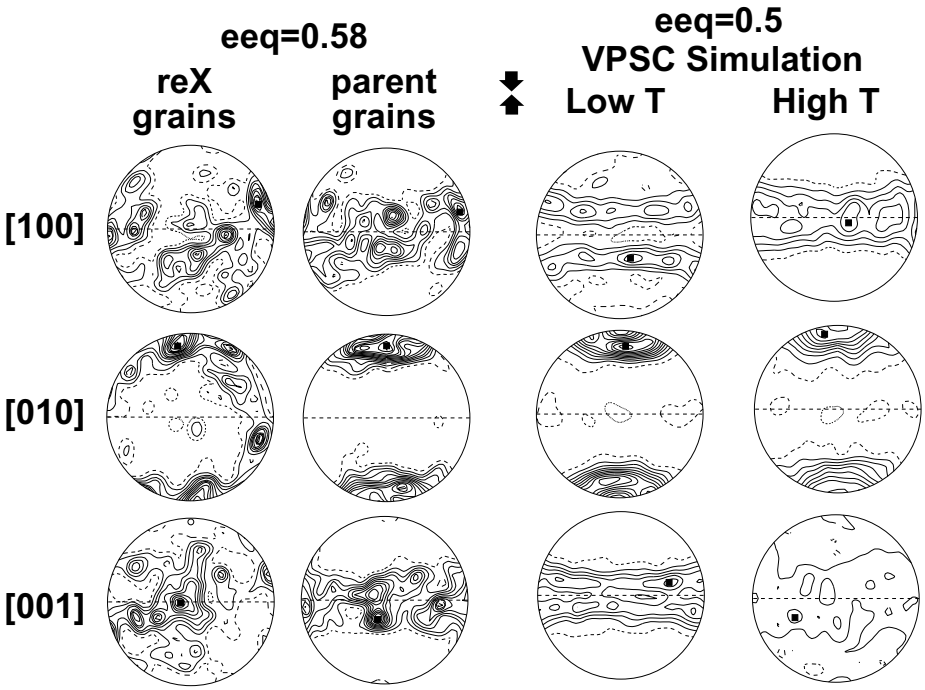

FIG. 3. Olivine lattice preferred orientations developed under axial compression. Left: experimental deformation of NICOLAS *et al*. (1973) for recrystalized (reX) and original (parent) grains. Equivalent strain is 0.58. Right: Simulations at equivalent strains of 0.5. Anisotropic VPSC (viscoplastic self-consistent, see text) fully constrained model, low and high-temperature critical resolved shear stress (CRSS). Equal area projections, lower hemisphere; 1000 grains, contours at 0.5% intervals. Dotted line: foliation plane, lineation direction is in foliation plane and in the plane of the figure. Full squares indicate maximum values, open circles minimum values. Arrows give compression direction.

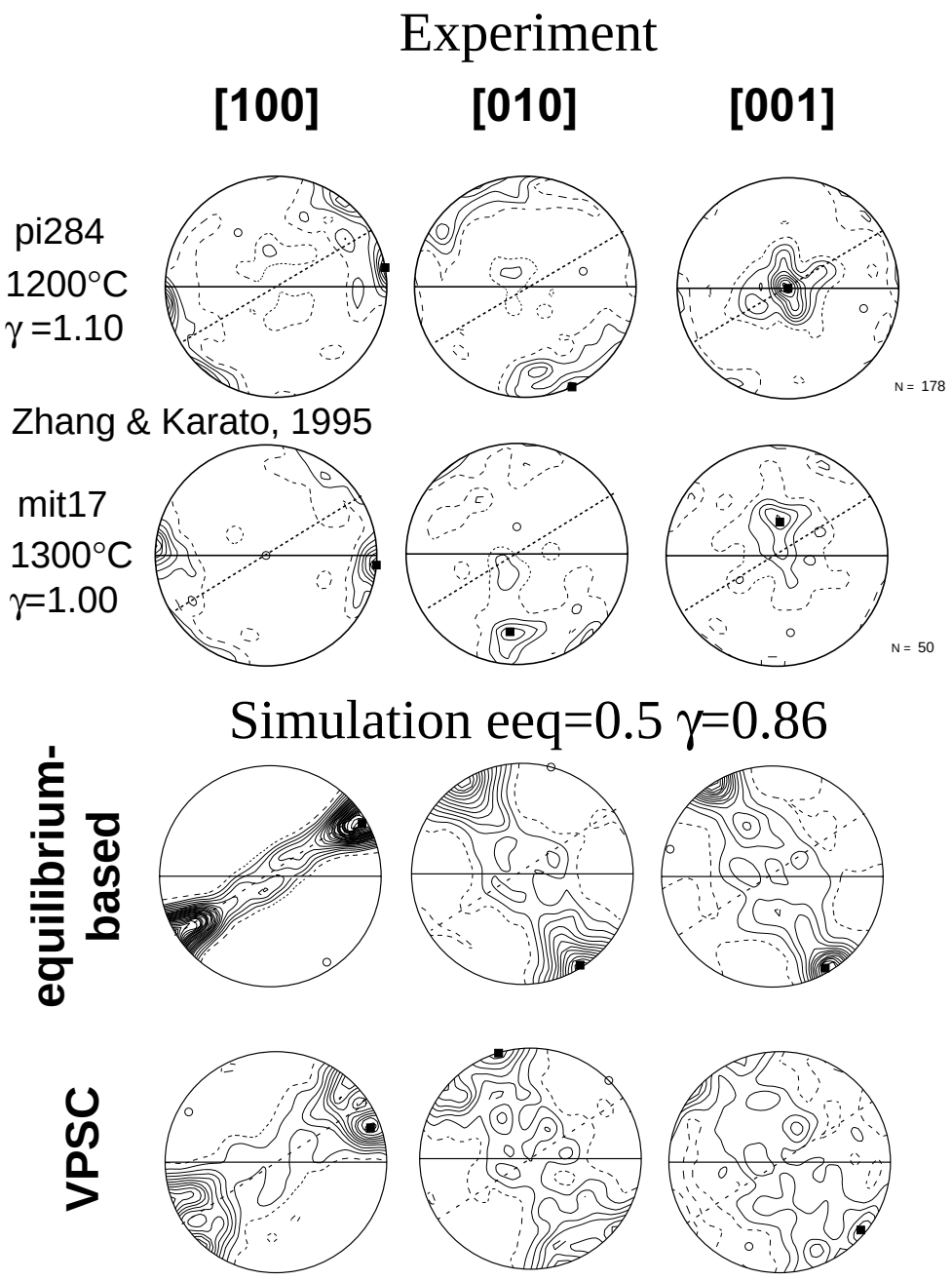

FIG. 4. Olivine lattice preferred orientations developed in dextral simple shear. Top: experimental simple shear deformation of olivine aggregates at 1200° and 1300°C (ZHANG and KARATO, 1995, pi284 and mit17 are sample names). Simulations at equivalent strain of 0.5 anisotropic VPSC and in an equilibrium-based model. Equal area projection, lower hemisphere; 1000 grains, contours at 0.5%. Solid line: shear plane, dotted lines, foliation plane, Lineation parallel to trace of foliation plane. Full squares indicate maxima in axis concentration.

at 1300°C display an LPO pattern characterized by a much faster rotation of [100] and [010] into parallelism with the shear direction and the normal to the shear plane respectively (Fig. 4). These samples differ from those deformed at 1200°C by a higher degree of dynamic recrystallization by subgrain rotation and grain boundary migration (>80% for a specimen submitted to a shear strain of 1.5). This suggests that in simple shear, dynamic recrystallization processes not only affect LPO intensity, but also modify the pattern, leading to a single LPO maximum in which the main slip system parallels the macroscopic shear.

Numerical experiments. The evolution of LPO in deforming olivine polycrystals has been studied by numerical methods, using several different approaches. The first is the purely kinematic method which only accounts for the geometrical aspects of glide and crystal rotation (ETCHECOPAR, 1977; ETCHECOPAR and VASSEUR, 1987; RIBE, 1989). Other methods take into account both the geometrical and mechanical aspects of the problem. There are a spectrum of possible mechanical solutions involving the compatibility of stress and strain fields in the aggregate. There is the homogeneous strain solution of TAYLOR (1938), which requires 5 independent glide systems, and consequently represents the upper bound of mechanical strength. The homogeneous stress solution with no strain compatibility of CHASTEL *et al*. (1993) constitutes the lower bound. Olivine has only 3 independent glide systems so that the Taylor model is not strictly applicable, but a Taylor model with relaxed constraints has been used in which particular components of the single-crystal strain tensor are allowed to differ from the aggregate strain tensor (TAKESHITA, 1989; TAKESHITA *et al*., 1990). Equilibrium-based methods (CHASTEL *et al*., 1993; BLACKMAN *et al*., 1996) make a stress-equilibrium assumption with relaxed strain compatibility. The isotropic (TAKESHITA *et al*., 1990; WENK *et al*., 1991) and anisotropic (TOMMASI *et al*., 1999) viscoplastic self-consistent (VPSC) approaches use the Eshelby inclusion method to take into account grain interaction, an important factor in the elasticity and plasticity of polycrystals. This self-consistent approach represents a compromise between stress and strain compatibility and hence is between the upper bound and lower bounds in mechanical strength. In practice, this approach is closer to the lower bound, implying that stress equilibrium is favored over strain compatibility. The mechanically based models of CHASTEL *et al*. (1993), BLACKMAN *et al*. (1996), TAKESHITA *et al*. (1990), WENK *et al*. (1991), and TOMMASI *et al*. (1999) assume a viscoplastic macroscopic response (termed viscoplastic selfconsistent or VPSC models) or where the crystals obey a power law between strain rate and stress, which is more appropriate for silicates deforming at high temperature than the elasto-plasticity of Taylor type models.

The LPO predicted by different polycrystalline plasticity models agrees, to first order, with experiments. However, simulated and measured LPO patterns differ in their relative organization of the [100] and [001] axes. In the case of the axial compression experiments, [001] axes form a girdle almost normal to the shortening direction, whereas the [100] axis distribution is more diffuse (Fig. 3). In simulations, [100] orientations are concentrated in a girdle normal to the compression direction and [001] orientations show a more diffuse distribution. This discrepancy between observed and modeled LPO may be explained by activation of different slip systems in models and experiments due to the high stresses involved in the experimental deformation.

LPO formed in simple shear at 1200°C exhibits good agreement with model predictions; both yield an orthorhombic pattern that results from dominant slip on (010)[100] (Fig. 4). The anisotropic VPSC model predicts a clear bimodal LPO pattern with the [100] peak intermediate between the shear direction and the finite elongation direction (X). Equilibrium-based models are less effective in reproducing the experimental results; they predict a single [100] maximum parallel to the lineation. Yet, even in the best models a few differences persist. Simulations predict a clear bimodal LPO pattern whereas LPO of experimentally sheared dunites display a dispersion of both [100] and [010] within the XZ plane. This dispersion may result from the activation of dynamic recrystallization by subgrain rotation which is not simulated. At a given strain, experimental samples display a greater concentration of [001] than predicted by anisotropic VPSC models. This could be explained by a lower activation of slip on (001) planes in the experiments.

The experimental work and numerical models have established that strength of LPO is a function of finite strain, and hence the seismic anisotropy should evolve with deformation history. To quantify the degree of LPO MAINPRICE and SILVER (1993) used the *J* index, which is defined as

$$J = \int f(\boldsymbol{g})^2 \, dg$$

where $\boldsymbol{g}$ is the crystal orientation and $f(\boldsymbol{g})$ the distribution of orientations. The *J* index has a value of unity for random LPOs. MAINPRICE and SILVER (1993) showed that the *J* index and the seismic anisotropy increased with increasing axial shortening of olivine aggregates by using the experimental data of NICOLAS *et al*. (1973). Numerical models of LPO (TOMMASI *et al*., 1999) as well as the analysis of ZHANG and KARATO (1995)

data confirm that the *J* index increases with finite strain (Fig. 5).

Thus, although the effects of recrystallization on LPO warrant further study, the patterns produced by the simulations are sufficiently good to capture the essentials of the seismic anisotropy for geodynamic modeling. Both anisotropic VPSC models with variable grain shape (TOMMASI *et al*., 1999) and hybrid constrained simulations (RIBE and YU, 1991) predict LPO patterns that are in good agreement with those observed in simple-shear experiments at 1200°C. Dynamic recrystallization will induce a faster rotation of LPO, resulting in a single maximum LPO characterized by parallelism between (010)[100] and the macroscopic shear. Yet, LPO patterns are similar and the angular misorientation between modeled and measured LPO is usually less than 20° in anisotropic VPSC with relaxed strain compatibility. Thus, we suggest that these simulations provide reasonable first-order predictions of LPO development during simple-shear deformation in the upper mantle. Moreover, although equilibrium-based models (CHASTEL *et al*., 1993; BLACKMAN *et al*., 1996; BLACKMAN and KENDALL, 1997) produce olivine pole figures that are less consistent with the experimental or natural ones, compared to the more computationally demanding self-consistent method (TOMMASI *et al*., 1999; see Figs. 3 and 4), there is little difference between the predicted seismic properties by these methods. Seismic anisotropy is sensitive to the general statistical properties of crystal orientations, rather than the details of individual pole figures.

The direct mantle sample: importance of mantle nodules.

Probably the most direct information about the deformation of aggregates comes from analysis of mantle samples that arrive at the surface by a variety of processes. These samples include ophiolites, and nodules brought to the surface by subduction zone and kimberlitic eruptions. The most appropriate for studying the subcontinental mantle are of course the kimberlite nodules. The first paper to consider their seismological properties was that of MAINPRICE and SILVER (1993), who analyzed the petrofabrics of a suite of 5 kimberlites. These 5 samples were chosen

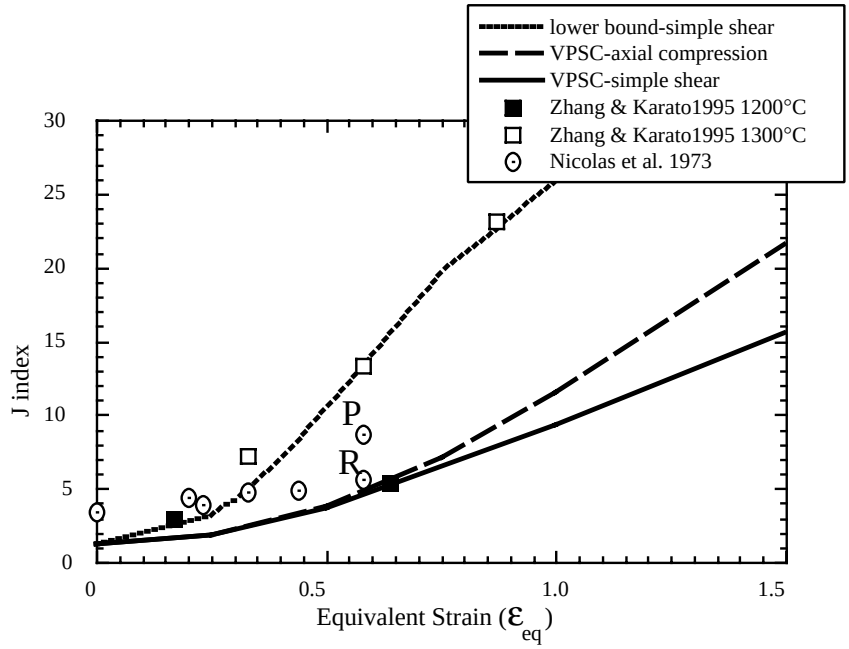

FIG. 5. Evolution of LPO intensity (represented by the *J* index, i.e., the integral of the Orientation Distribution Function, *e.g.*, MAINPRICE and SILVER,1993) as a function of the equivalent strain for anisotropic VPSC models in axial compression, pure shear, and simple shear with α = 1, 10, or 100 and for NICOLAS *et al.* (1973) axial compression experiments (full circles: porphyroclasts, open circle: recrystallized grains).

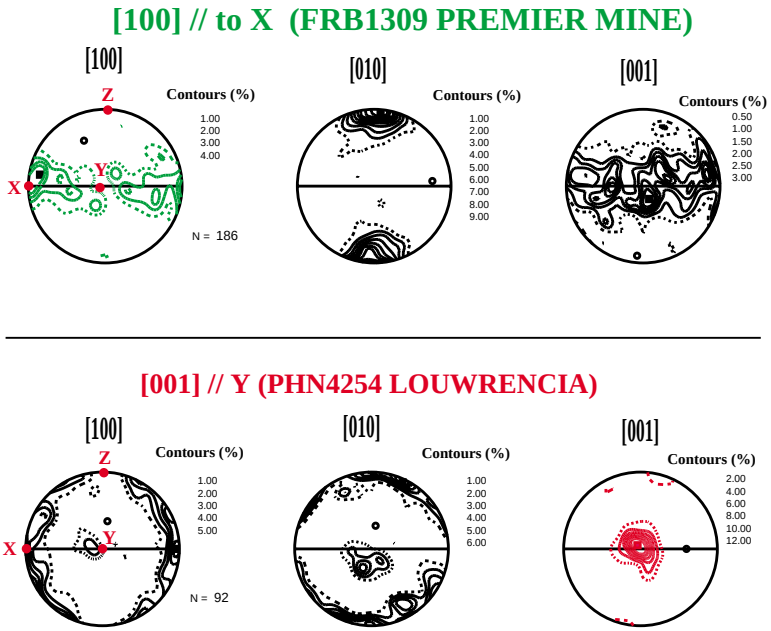

FIG. 6. Olivine pole figures for [100], [010] and [001], for two mantle nodules from lithosphere beneath Kaapvaal craton in Africa. Such diagrams illustrate the degree to which crystalographic axes are concentrated in particular directions. Contours of concentration, expressed as percent greater than a uniform distribution, are shown the the structural frame, defined by X=lineation direction Z=normal to the foliation plane (horizontal line is trace of foliation plane) and Y= normal to X in foliation plate.

as representative of the lithosphere in the depth range of 120-170 km based on geobarometry. They appear to be undisturbed by the eruption process (in contrast to the sheared nodules). The elastic properties of the aggregates were determined by petrofabric analysis of the samples, knowledge of the single-crystal elastic constants and their temperature and pressure derivatives. The analysis of these samples allows the aggregate elasticity matrix to be placed in a structural frame. This characterization of the elasticity matrix and its placement in the structural frame is perhaps the most important step in the interpretation of seismic anisotropy, as it provides the critical link between orientation of deformation and orientation of anisotropy. In this initial study, 5 such samples were averaged in the structural frame. Such an average would be appropriate for seismic waves as long as the deformation is spatially coherent. It is thus an upper bound on the actual detectable anisotropy. In that study it was found that the maximum shear-wave anisotropy was 3.7%, while anisotropy for propagation along the three structural directions yielded 1.7%, 3.1%, and 1.6% for the *X*, *Y*, and *Z* directions, respectively. For vertical propagation, if the foliation is plane horizontal, as would be the case for asthenospheric flow, then the expected anisotropy is 1.6%, while a vertical foliation plane and horizontal lineation direction would yield 3.1%.

Recently, there has been an intense effort, in conjunction with the Kaapvaal Craton Experiment (CARLSON *et al.*, 1996) to examine a much larger group of mantle nodules, in order to assess the magnitude and orientation of the macroscopic seismic anisotropy, and to look for both lateral and vertical variations in anisotropy beneath the Kaapvaal craton and surrounding areas. Thus far, an order of magnitude more samples have been examined. The majority of them possess a fabric and intensity of anisotropy consistent with the Mainprice and Silver study (*e.g.*, sample FRB1309 Premier Mine, from JOE BOYD's collection, Figs. 6 and 7). There is, however, a second class of fabrics, making up roughly 25% of the data set with completely different characteristics, namely a strong concentration of [001]-axes parallel to the *Y* direction, i.e., the direction normal to both to the lineation direction and the normal to the foliation plane (*e.g.*, sample PHN4254, from PETER NIXON's collection, Figs. 6 and 7). The LPOs like PHN4254 produce a V_p maximum parallel to the lineation (*X*) and V_p minimum parallel to the foliation normal (*Z*), like the patterns previously reported by MAINPRICE and SILVER (1993). However, the V_s distribution is very different (Fig. 7), with a maximum shear wave splitting anisotropy of 0.16 km/s (A=3.2 %), parallel to the foliation normal (*Z*) rather than

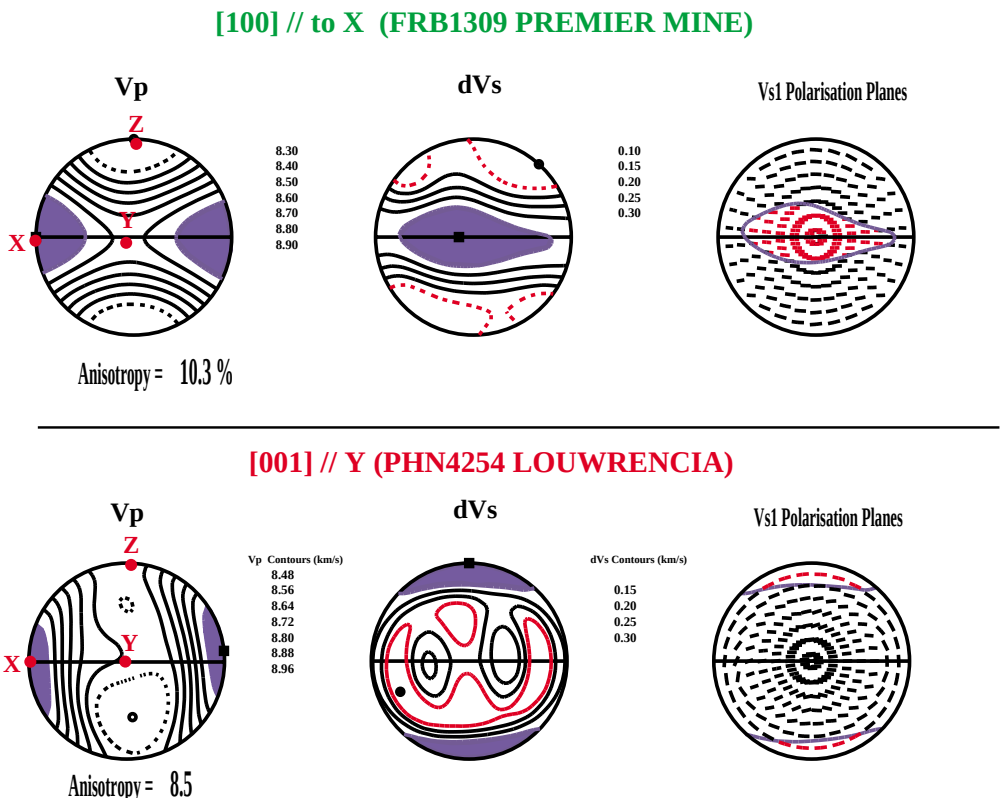

FIG. 7. Olivine seismic anisotropy corresponding to the LPO given in Fig. 6. Contours for V_p and dV_s in km/s. Trace of the V_{s1} polarization planes shown (right) as well as 0.3km/s anisotropy contour.

parallel to *Y*. For most propagation directions, the fast polarization direction is still parallel to the foliation plane as for the average sample of MAINPRICE and SILVER (1993), but for waves propagating parallel to the lineation direction, the fast polarization direction is normal to the foliation plane (Fig. 7). If an average of 33 Kaapvaal Craton samples is taken, using the LPO of olivine and enstatite (orthopyroxene), the resulting anisotropy is somewhat weaker than that reported by MAINPRICE and SILVER (1993) (Fig. 8). In the case of propagation along the *Y* structural direction, appropriate for vertical propagation with vertical foliation direction and horizontal lineation (the probable structural orientation for transpressional deformation, see next section), then the polarization is still parallel to the *X* direction, but the splitting anisotropy is reduced to about 2.2% (δV_s=0.12 km/s), or about 2/3 of the 3.1% value estimated by MAINPRICE and SILVER (1993) for the same direction. If we use this value, in conjunction with the estimated 0.65 s average splitting delay time for the Kaapvaal craton (GAO *et al.*, 1998), then it corresponds to a layer thickness of about 130 km. Allowing 40 km of crust (assumed isotropic), this brings the bottom of this layer to a depth of 170 km.

An interesting feature of the average elasticity matrix is that it predicts a much larger anisotropy, about 3.2% to 4.0% (δV_s = 0.16 - 0.20 km/s) for propagation along *Z*. This would correspond to horizontally propagating waves, like surface waves, as long as the structural frame is that expected for transpressional deformation, namely vertical foliation plane and horizontal lineation direction (Fig. 8). We note that constraints on S-wave anisotropy based on polarization anisotropy in horizontally propagating waves (SALTZER *et al.*, 1998) for the Southern African seismic experiment are in the range of 4-5% down to a depth of about 200 km and thus much larger than that inferred from the SKS splitting, assuming the previous estimates of continental anisotropy. This apparent discrepancy has been attributed to vertical heterogeneity (layers with [100] directions randomly distributed in the horizontal plane, SALTZER *et al.*, 1998), although the amount of vertical heterogeneity required is extreme (roughly 10 independent layers, see RUMPKER and SILVER,

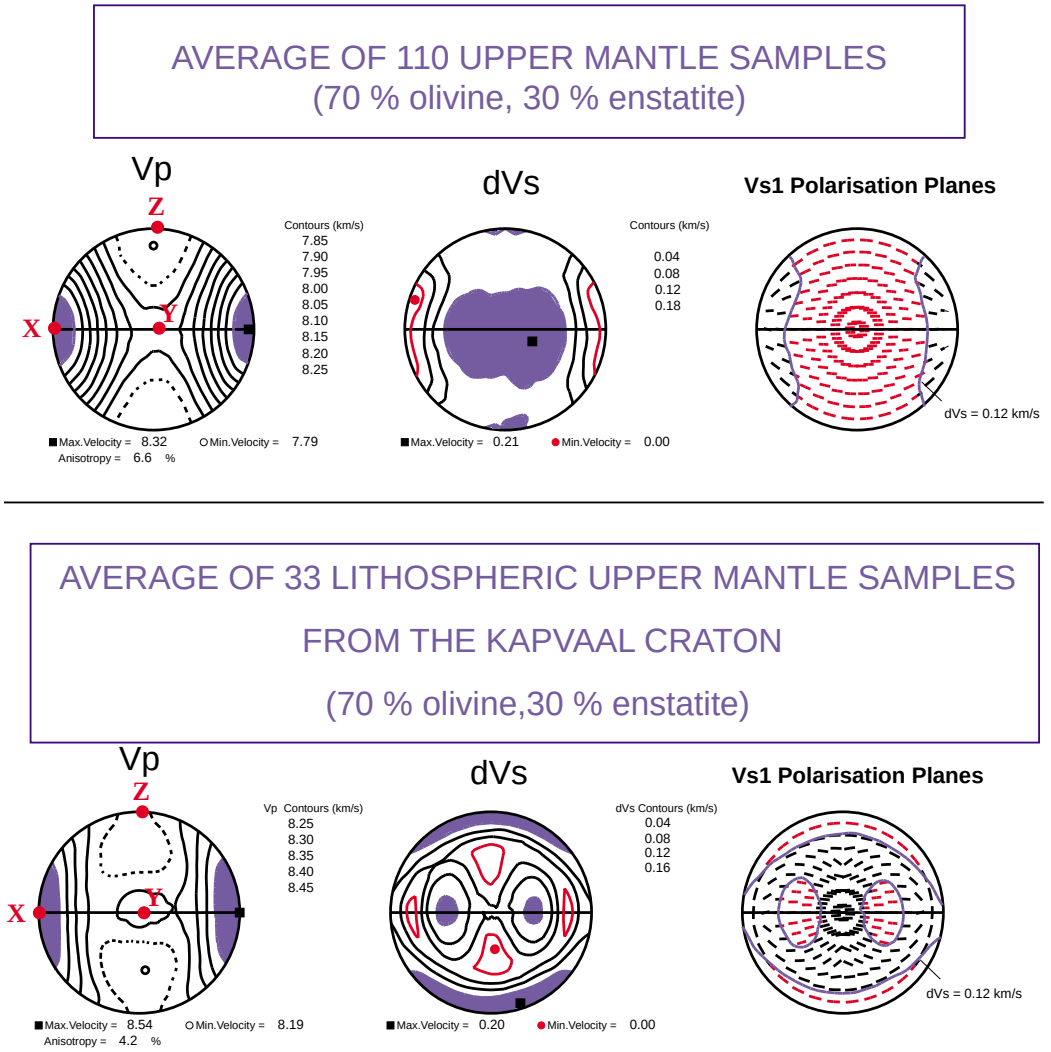

FIG. 8. Seismic anisotropy corresponding to the LPO given by the database of Ben Ismaïl and Mainprice (1998) for 110 upper mantle samples (top) and 33 samples from the Kaapvaal Craton (bottom, this work) for equivalent compositions of 70% olivine and 30% enstatite. Contours for V_p in km/s (left), δV_s in km/s anisotropy (center). Right, orientation of polarization planes for fast shear wave (V_{s1}), along with δV_s=0.12km/s contour line. Top figure does not include Kaapvaal samples.

1998), and such heterogeneity is in marked contrast to the close correspondence between the splitting fast polarization directions and the surface geology (GAO *et al*., 1998). The average elasticity matrix provides a simpler means of reconciling the two data sets, as long as the transpressional structural frame (foliation plane vertical, lineation direction horizontal) is the correct one. Since there appears to be no specific spatial distribution of this [001] concentration in the Kaapvaal data thus far (found at all depths and nearly all locations), then on the scale of seismic waves, the mantle beneath the Kaapvaal craton should appear as the average elasticity matrix calculated from the suite of samples.

BEN ISMAÏL and MAINPRICE (1998) have recently published a database for olivine LPOs that provides a means of comparing kimberlite nodules to mantle samples from other tectonic environments. When we compare the average seismic properties for olivine calculated for samples from fast spreading ridges (ophilolites) and xenoliths from subduction zone volcanism (BEN ISMAÏL and MAINPRICE, 1998) with South African kimberlite nodules (Fig. 9), we find that the P-wave anisotropy pattern is the same in all three cases. The S-wave pattern is the same for

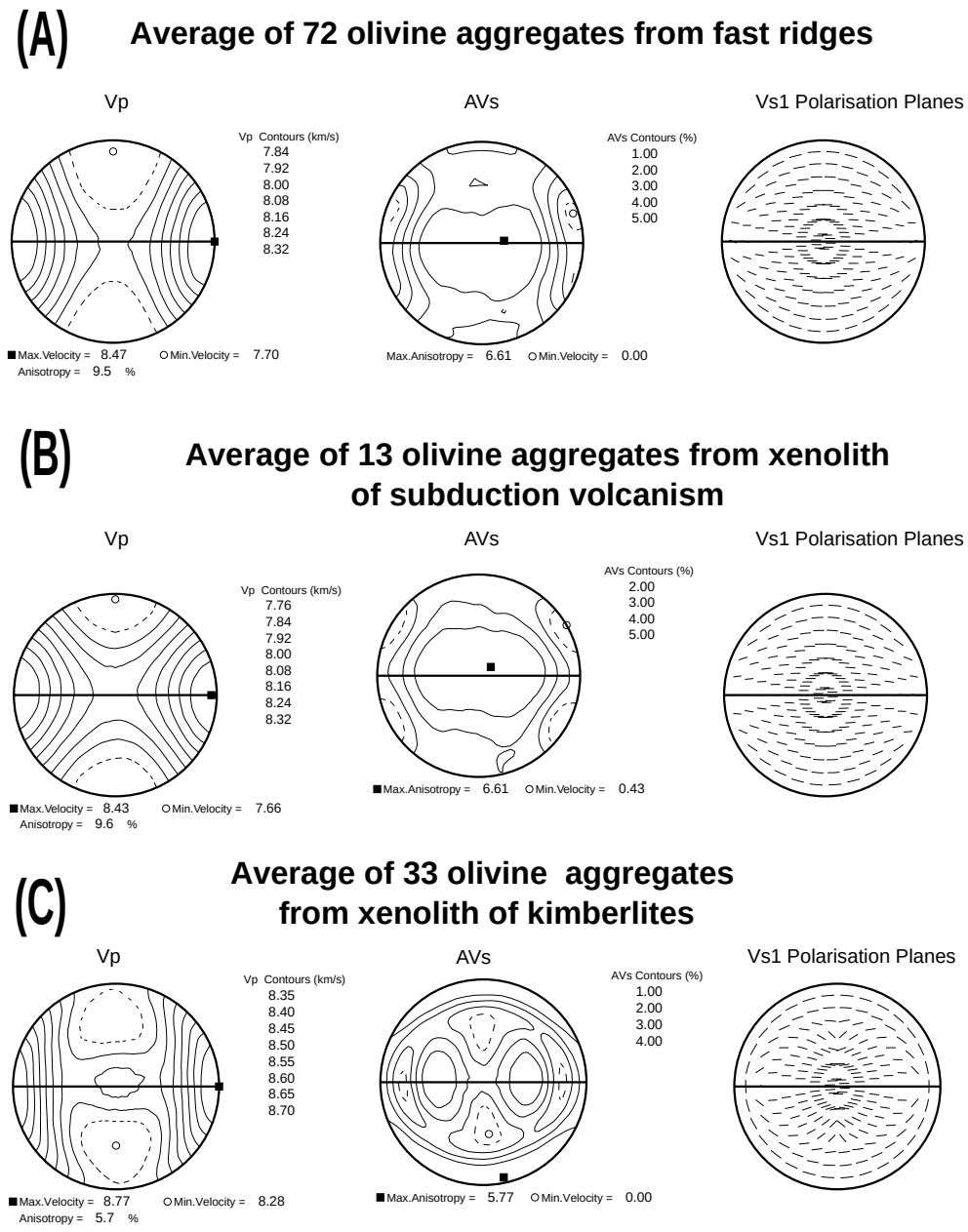

FIG. 9. Seismic anisotropy corresponding to the olivine LPO given by the database of BEN ISMAÏL and MAINPRICE (1998) for (a) fast ridges , (b) subduction zone samples and (c) Kaapvaal Craton (this work). Contours for V_p in km/s, δV_s in % anisotropy and trace of the V_{s1} polarization plane.

fast ridge and subduction zone environments, but different for the kimberlite suite. The V_p anisotropy is 9.5%, 9.6% and 5.7% for fast ridge, subduction zone, and kimberlite environments, respectively. The maximum V_s anisotropy is 6.6%, 6.6%, and 5.8% for fast ridge, subduction zone and kimberlite environments, respectively. The anisotropy pattern and magnitude show that the sub-continental mantle

suite from South Africa is significantly different from the oceanic environment represented by fast ridge and subduction zone samples.

BEN ISMAÏL and MAINPRICE (1999) have recently established an orthopyroxene LPO database as well. Although for olivine it is straightforward to measure 100 or more crystals in a thin section to obtain a reliable measure of LPO, the low volume fraction (typically 30%) of orthopyroxene makes this often impossible. BEN ISMAÏL and MAINPRICE (1999) have developed a method to weight the LPO so that it is independent of the number of grains measured. Using this method, the orientations from the olivine and orthopyroxene databases were used to calculate the variation of seismic anisotropy with LPO strength (Fig. 10). The relation between LPO strength and seismic anisotropy is non-linear for both olivine and orthopyroxene, with a steep increase in anisotropy at low *J* index followed by a slower increase above a *J* index of about 12. We note that olivine is two to three times more anisotropic than orthopyroxene for a given value of LPO strength. Much of this difference is due to the weaker single-crystal elastic anisotropy of pyroxene. In addition, olivine polycrystals can develop very strong LPO that have nearly single crystal anisotropy. Orthopyroxene polycrystals, on the other hand, never exhibit more than half the single crystal anisotropy and in general are characterized by weaker LPO (*J* = 1 to 10). In the database, the weakest olivine LPO has about *J*=4. There is a group of olivine fabrics from South African kimberlites with fabrics like PHN4254 (Fig. 6) which have an almost constant seismic anisotropy (ca. 9% for V_p) despite a *J* index that varies from 12 to 20. In naturally deformed peridotites there are no reliable markers of finite strain. If we take the *J* values of the olivine samples (about 5-25) and compare that with

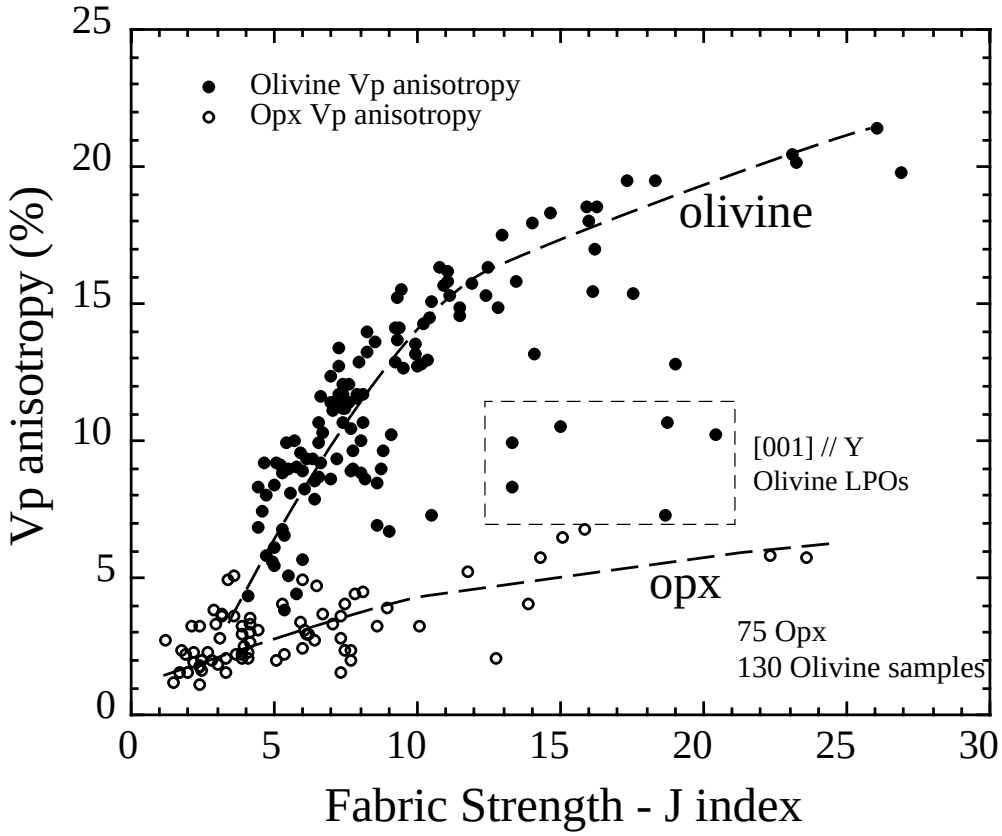

FIG. 10. seismic V_p anisotropy (%) for the olivine and orthopyroxene databases as a function of LPO intensity (defined by the J index). The olivine values in the black box are fabrics with a strong c-axes maximum parallel to Y such as PHN4254 in Fig. 6. Trend lines are there to indicate tendencies and are not fitted functions.

the LPO evolution in numerical simulations or experiments in simple shear (Fig. 5), then apparently the LPO of naturally deformed peridotites is recording a shear strain of γ between 0.8 and 2.5 with the majority being close to 1.7. One would expect that these rocks have suffered much higher shear strains than 2.5 (especially for asthenospheric flow) and the most plausible reason for the low values is that dynamic recrystallization reduces LPO intensity, leading to constant J values during deformation. Indeed, the recrystallized grains in the experiments of NICOLAS *et al*. (1973) have weaker LPO than porphyroclasts (Fig. 5). However, effects such as grain boundary migration may increase the LPO strength; for example, the strongest fabrics in the olivine database come from dunite samples with strong grain growth microstructures. The strongest fabrics from ZHANG and KARATO's (1995) simple shear experiments on pure olivine aggregates at 1300°C also show evidence of grain boundary migration. In most natural samples, the presence of other minerals (orthopyroxene, garnet, clinopyroxene, *etc*.) will inhibit extensive grain boundary migration. It would thus seem likely that dynamic recrystallization by a mechanism such as sub-grain rotation would cause the LPO intensity and hence, the seismic anisotropy to saturate. Numerical simulation models that take into account recrystallization (*e.g.*, WENK *et al*., 1997) need to be applied to olivine. If we take the value of anisotropy at the change in slope of anisotropy versus J index as the stabilized or saturated value, then the database indicates that this occurs at about 0.6 of the anisotropy of the single crystal value for olivine and 0.35 for orthopyroxene.

The trend of anisotropy versus LPO strength shown is Figure 10 for olivine and is essentially defined by the oceanic samples. The LPO pattern in oceanic samples agrees well with deformation experiments and numerical simulations in simple shear (Fig. 4), indicating that these oceanic LPO patterns are essentially due to simple shear deformation at moderate to high temperature. The sub-continental mantle LPOs from South Africa, however, show a strong deviation from this trend, particularly the patterns in samples like PHN4254. The most probable explanation for this difference is that these sub-continental mantle samples have had a long period of residence within the lithosphere after deformation, perhaps hundreds of millions of years, at mantle conditions of 100 to 150 km depth and 1000°C (BOYD, 1973), during which time processes like abnormal grain growth (HUMPHREYS and HATHERLY, 1995) have altered the LPO pattern. Abnormal grain growth occurs when there is a local destabilization of the grain structure by the removal of a pinning point (*e.g.*, a small grain or fluid inclusion on a grain boundary, say 5 times smaller than the average grain size), leading to inhomogeneous growth with a few grains growing excessively at high temperature. All of these samples are characterized by large grain sizes, probably their only common feature.

Some basic conclusions can be drawn from this statistical approach to mantle LPO and seismic anisotropy: (i) A significant difference in anisotropy and LPO pattern exists between the sub-continental mantle of South Africa and oceanic mantle. In part, this difference may be due to its Archean age, a period with a very different geothermal regime. (ii) Oceanic mantle has a stronger anisotropy than sub-continental mantle. (iii) The strain recorded by LPO in upper mantle samples (and hence observable seismically) corresponds to a shear strain of less than γ =2 and hence only the last increment of mantle deformation is observable. (iv) The South African sub-continental samples are characterized by larger grain size, and weaker LPO and anisotropy than oceanic samples. The long period of residence after deformation of sub-continental samples at 1000°C has apparently allowed a weakening of LPO, most probably by abnormal grain growth.

PREDICTING THE DEFORMATION FIELD FOR VARIOUS TECTONIC PROCESSES

In order to ultimately relate observations of seismic anisotropy to the various tectonic processes that deform the mantle, it is necessary to predict the deformation field that the process will create. With this relationship in place, it is then possible to perform tests of dynamic models, based on anisotropic observations. Rather than treat this problem in general, we consider two sources of mantle deformation that would be expected to be present in the subcontinental mantle. The first, simple asthenospheric flow (SAF) (Fig. 11) is based on the idea, developed first for oceanic plates, that the velocities of the surface plates are much greater than that of the deeper mantle, and that there exists a mechanical decoupling zone (decoupling the plates from the mantle below) usually referred to as the asthenosphere, that concentrates strain. The second is vertically coherent deformation (VCD) (Fig. 11), which simply assumes that the crustal and mantle portions of plates deform coherently.

In the case of simple asthenospheric flow, the flow field and corresponding anisotropic properties are straightforward to predict. We assume that the foliation plane and lineation direction are both horizontal and that the lineation direction follows the flow line, which in turn is parallel to the absolute plate motion (APM) direction of the plate. We furthermore assume, based on the discussion in the previous section, that the memory of asthenospheric flow direction is short, only a few million years, since strains of order unity, enough to

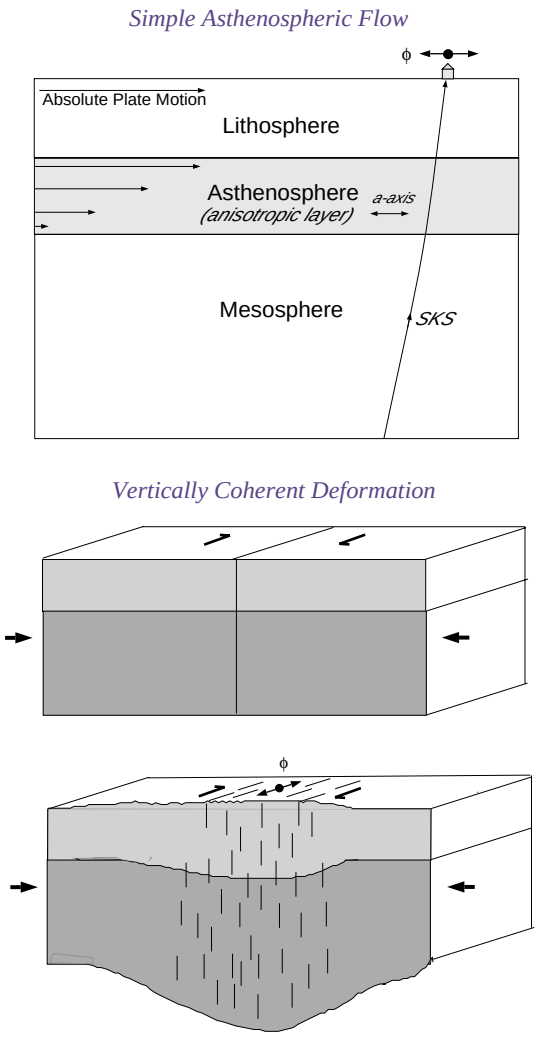

FIG. 11. Hypotheses for the development of seismic anisotropy: (top) Simple Asthenospheric Flow (SAF) and (bottom) Vertically Coherent Deformation (VCD).

completely reorient olivine aggregates (NICOLAS *et al*., 1973, see also MAINPRICE and SILVER, 1993; CHASTEL *et al*., 1993), will be generated in that amount of time for the range of plate speeds (1-10 cm/yr), and an asthenospheric thickness of order 100 km (Fig. 11). For vertically propagating shear waves, the predicted direction of ϕ, ϕ_{apm}, is then parallel to the APM direction. Even if the APM direction is poorly known, as in the case of Eurasia, (MINSTER and JORDAN, 1978; GRIPP and GORDON, 1990), the dominance of asthenospheric flow would reveal itself as coherent directions that could be characterized by a single pole of rotation. Thus, for plates with well known APM directions, one can simply compare observed with predicted values or, more generally, test for large-scale coherence of fast polarization directions. This may be done on a point-wise basis over the plate, or by testing for variations in splitting parameters on regional length scales (less than 1000 kilometers) where the SAF component should be constant. Significant variations in ϕ on a regional scale constitute a basis for rejecting the SAF hypothesis as the dominant source of mantle anisotropy. Of course, there is the possibility of more complex asthenospheric flow patterns. For example, significant relief in the lithosphere-asthenosphere boundary could induce local variations in the asthenospheric flow direction (BORMANN *et al*., 1996; BARRUOL *et al*., 1997; FOUCH *et al*., 1999), or alternatively, small-scale convection may be present. It is, however, useful to distinguish between simple asthenospheric flow, the idealized form of asthenosphere beneath oceanic lithosphere, and these more complex flow models.

The hypothesis of vertically coherent deformation (SILVER and CHAN, 1988; 1991; SILVER, 1996), states that continental plates deform coherently over their depth extent. It is additionally hypothesized that the last significant penetrative episode of orogenic deformation controls the mantle anisotropy (consistent with the results of the previous section), whether the event is occurring today or occurred in the Archean. This hypothesis predicts that spatial variations in splitting parameters should track variations in crustal deformation, based on structural geological or tectonic studies (Fig. 11).

In principle, there are three major categories of deformation that would be encountered: transcurrent, collisional, and extensional regimes. In fact, pure collisions are rarely observed, and there is almost always a significant transcurrent component (VAUCHEZ and NICOLAS, 1991), usually referred to as transpression. For transcurrent deformation, we assume that the foliation plane is vertical and the lineation direction is horizontal and parallel to the transcurrent structure (approximate for large strain), in which case ϕ is also parallel to the transcurrent structure. For transpression, we again assume that the foliation plane is vertical, but that the lineation direction may be significantly different from horizontal. As long as it is not vertical, however, ϕ will, like transcurrent motion, still be parallel to transpressional features. Even for non-vertical propagation directions within the foliation plane, ϕ is still approximately parallel to the lineation direction, as indicated by Fig. 7. Because extensional regions make up a much smaller component of the splitting data set, and because they are more difficult to interpret (SILVER, 1996), we will focus our attention on the transpressional environments.

INTERPRETATION OF THE SPLITTING DATA SET

After more than a decade of accumulating over 400 shear-wave splitting observations, it has become increasingly clear that for transpressional zones, the dominant source of mantle anisotropy is vertically coherent deformation of the continental plate (SILVER, 1996). This basic conclusion allows us to use seismic anisotropy to extend our understanding of the geology of surface tectonic processes, especially structural geology, into the mantle. The mantle's role in orogenies in particular, and the evolution of continents in general, can thus be assessed. Equally important for ancient orogenic episodes is that the anisotropy, and hence information about mantle deformation, is preserved, as long as it is not overprinted by a subsequent episode. Vertically coherent deformation is observed in most stable continental areas of all ages, and is also seen in presently active regions. There are zones that deviate from this general conclusion, however. Tectonic North America (from the Rocky mountains to the west coast) in particular reveals a complex pattern of anisotropy that cannot be easily related to the surface geology or to simple asthenospheric flow that would be created by the North American plate passing over a slowly moving mantle. Stable North America (east of the Rocky mountains) possesses values of ϕ that are parallel to APM as well as local geology. This presents an ambiguity that is difficult to assess. It has recently been argued, in fact, that the splitting pattern for stable North American can be partially explained by flow around a continental keel (BARRUOL *et al*., 1997; FOUCH *et al*., 1999). The only difficulty with this model is that the largest values of splitting are observed where the lithosphere is thickest, suggesting that a large portion of the anisotropy is in the lithosphere. It still may be that present-day shear deformation of the root is responsible for some of the fabric. The general conclusion remains, however, that vertically coherent deformation is the dominant contribution. We give three examples from different geological periods that illustrate this conclusion, from the Paleozoic, the Archean, and the present.

Eurasia is by far the largest continental land mass and has large stable regions that are ideal for hypothesis testing. One such region is central Europe. As shown in Fig. 12 there is a systematic variation in fast polarization directions on a regional scale. In particular, north of the Alpine deformation, stations show a systematic variation from roughly NE-SW in the west, to NW-SE in the east: a rotation of nearly 90° over 500 km (BORMANN *et al*., 1993 and VINNIK *et al*., 1994). This variation is unlikely to be caused by simple asthenospheric flow, because of the small spatial scales of deformation. We can furthermore test for possible coherence between splitting parameters and surface geology, since the structural geology is particularly well characterized. As noted by BORMANN *et al*. (1993), and as is clear from Fig. 12, this pattern follows the general trends of the Paleozoic Hercynian orogenic belt in this zone, as indicated by the orientation of fold axes (taken from BORMANN *et al*., 1993).

A second example is provided by data from a recent seismic experiment (Southern African Seismic Experiment) that has been conducted in part to measure the anisotropy beneath the early Archean Kaapvaal craton. This is a unique locale, since we also have additionally petrofabric control from the kimberlite nodules, as discussed above. The preliminary results from the analysis of splitting (GAO *et al*., 1998) is shown in Fig. 13, along with a structural map from DEWIT *et al*. (1992) giving the large-scale geological structures of the craton. Splitting has been detected at most stations, and there are systematic spatial variations in ϕ. The data may be separated into three geologic regions. First, there is the southern Kaapvaal group with values of ϕ trending NE-SW, a second group further north within the Limpopo belt with directions more nearly EW, and group of stations on the Zimbabwe craton with directions ranging from NE-SW to NNE-SSW. In all three regions, values of ϕ follow closely the orientation of Archean orogenic structures, a result that is consistent with vertically coherent deformation. Splitting delay times are small, averaging 0.65 s, compared to a global average of about 1s for continents worldwide. As noted previously, if we take the value of intrinsic anisotropy δV_s equal to 2.2%, assuming the structural frame is in the orientation appropriate for transpressional deformation, then the average thickness of the anisotropic region is inferred to be about 130 km. Assuming the crust does not contribute to the splitting, this places the base of the anisotropic zone near 170 km depth beneath southern Africa, an estimate that is close to the estimates of lithospheric thickness from the boundary between high-temperature and low temperature nodules.

A third example comes from Tibet, a plateau that was formed by the collision between the Indian and Eurasian plates. The results from an experiment along a north-south line in eastern Tibet (MCNAMARA *et al*., 1994), are shown in Fig. 14. For most of the line, especially the northern stations where the delay times are largest, there is a close correspondence between the orientation of the large-scale surface deformation and the orientation of ϕ. In particular, the anisotropy appears to record in the mantle both the shortening and extrusion of Tibet towards the east (see MCNAMARA *et al*., 1994 for

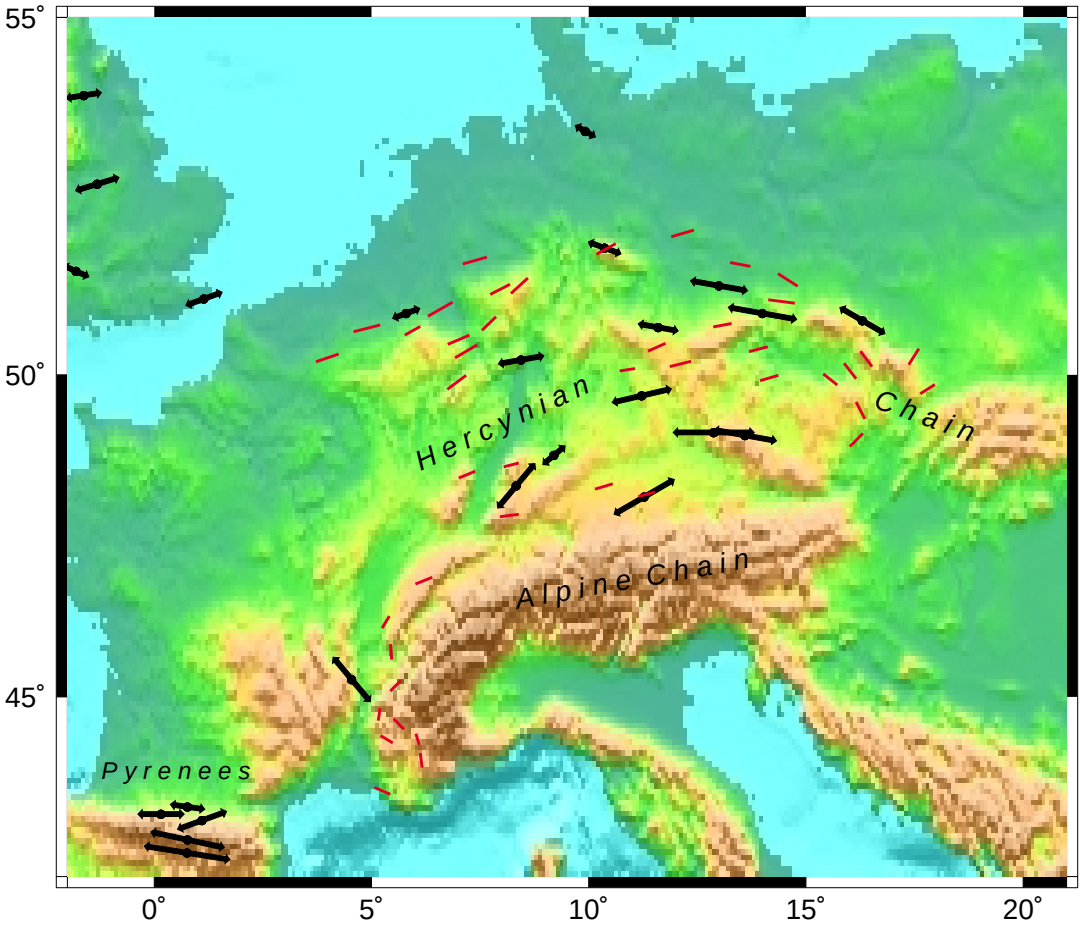

FIG. 12. Central Europe. Thick lines are splitting parameters. Short line segments denote fold-axis orientations for (Paleozoic) Hercynian orogenic belt, from compilation of BORMANN *et al*. (1993). Note significant variations in ϕ within Europe. This is inconsistent with SAF hypothesis. Note also close correspondence between fold axes and ϕ indicating coherent deformation between crust and mantle (from Silver, 1996).

discussion). The largest SKS delay time yet recorded (2.4 s) was observed at the northern edge of the Plateau, just south of the active strike-slip Kunlun fault. In the case of Tibet, it has been possible to do a particularly careful job of assessing the surface deformation and its correspondence to mantle deformation, because of the grand scale of the Tibetan deformation. Recently HOLT and HAINES (personal communication, 1999) have estimated a smoothed surface strain field for Tibet, based on the orientation and inferred slip on Quaternary faults, as well as by fault plate solutions. As shown in Fig. 14, there is a remarkable correspondence between the fast polarization directions of splitting, and the estimated orientation of the shear planes for left-lateral shear. This correspondence is explained if (i) the [100] axis of olivine follows the shear, rather than foliation plane for large strains, as was concluded in the experiments of ZHANG and KARATO (1995), (ii) the mantle strain field is very smooth, and (iii) there is strong coherence between crust and mantle deformation down to perhaps 300 km depth.

CONSEQUENCES OF ANISOTROPIC OBSERVATIONS

The pervasiveness of vertically coherent deformation beneath the continents leads to two important conclusions concerning the evolution of continents. First, there is little unambiguous sign of

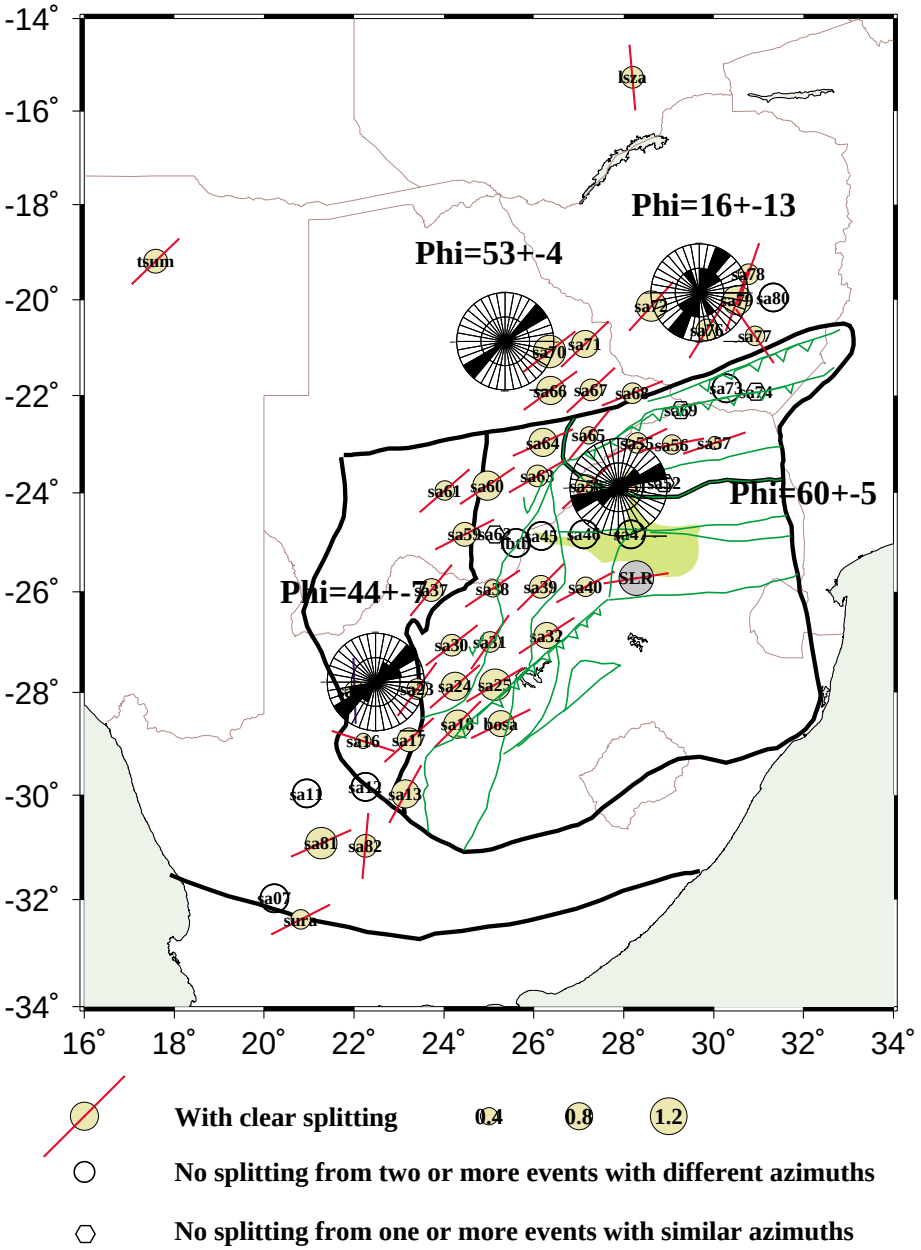

FIG. 13. Shear-wave splitting results from the Southern African Seismic Experiment (From GAO *et al.*, 1998). Numbers give the average values of ϕ for geologic subregions. Grey area denoted Bushveld igneous province. See text for details.

a continental asthenosphere that decouples the plate from the mantle below. This is a general feature of the stable regions of continents that have thus far been examined. Second, the dominance of vertically coherent deformation throughout Earth's history suggests that the orogenic process involves the deformation of the entire plate, a process that for collisions is expected to produce thickened mantle roots. Such a model accounts for the usually thickened crust, but, as we will see, does not easily

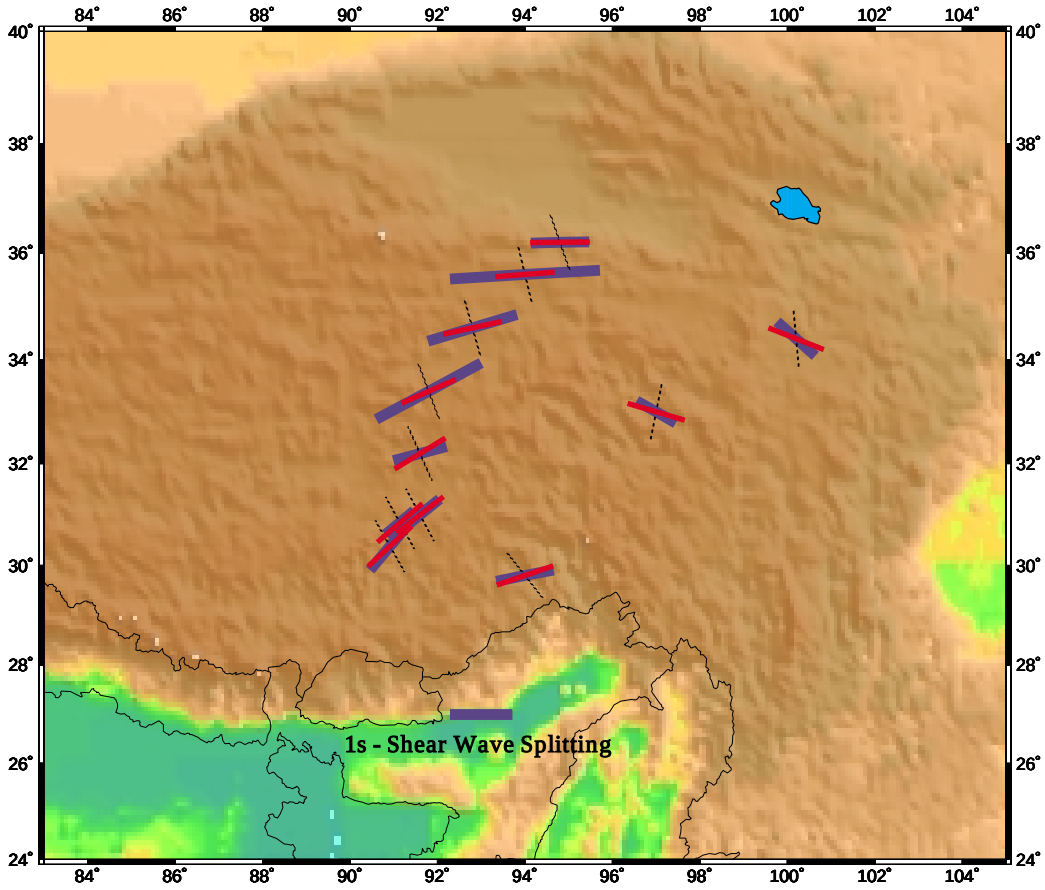

FIG. 14. Shear-wave splitting from Tibet. Black lines give shear-wave splitting parameters from MCNAMARA *et al*. (1994). Also shown, zero-length lines of finite strain ellipsoid from smoothed strain map of Tibet derived from slip on Quaternary faults (HOLT and HAINES, 1999, personal comm.). Solid gray and dashed black lines correspond to left- and right-lateral shear directions, respectively. Note the remarkable correspondence between orientations of fast polarization direction ϕ and left-lateral shear directions, consistent with the hypothesis of vertically coherent deformation between the crust and mantle during the formation of Tibet.

account for the high temperatures usually associated with orogenic crust and mantle.

Is there a continental asthenosphere?

There are three possible explanations for the apparently small contribution of a continental asthenosphere. First, the continental asthenosphere could be very thin, of order 10 km, and not produce a measurable anisotropic signal. Second, it may be that under the conditions found within the continental asthenosphere, anisotropy (namely LPO) is not developed. This would be the case, for example, if deformation took place by diffusion creep, rather than dislocation creep (*e.g.*, KARATO, 1992; 1993). The third explanation is that a continental asthenosphere is not present beneath continents. We take these possibilities in order. A very thin layer seems improbable, given the geometrical difficulties introduced by large (or order 100 km) variations in the depth to the base of the lithosphere. At a minimum such an asthenosphere would still permit strong coupling to occur, especially where there are abrupt changes in lithospheric thickness. The second possibility is a change in deformation mechanism from dislocation to diffusion creep at conditions where a continental asthenosphere is present. This problem is complicated in general, because the deformation mechanism depends on several physical variables, such as pressure, temperature, stress, grain size and concentration of contaminants, such as water. The

problem of asthenospheric conditions, however, is relatively well constrained. We have reasonably good evidence that lattice preferred orientation occurs in the oceanic asthenosphere. One line of evidence is from ophiolites, where the thermal properties, such as evidence of melt, suggest asthenospheric conditions near a spreading ridge (A. NICOLAS, personal comm.). Another data source is the shear wave splitting near mid-ocean ridges. The MELT experiment (WOLFE and SOLOMON, 1998) provided evidence for significant splitting for near-ridge sites. The observed orientation of ϕ parallel to spreading, strongly suggests that LPO in olivine is the mechanism for the splitting. The physical conditions for a continental asthenosphere would be very similar to the more shallow oceanic one: specifically, a similar temperature, defined by the base of the lithosphere and a similar strain rate, defined by plate velocity. The main difference is pressure, and this has two potentially important effects. First, according to KARATO (1992), diffusion creep should have a lower activation volume than dislocation creep, and should therefore be favored at higher pressure. On the other hand, viscosity, and hence stress should also increase with pressure (at constant temperature), which favors dislocation creep. If these two effects cancel each other out, then we would expect LPO to develop because it is observed at lower pressures. The absence of LPO requires then requires that diffusion creep possess a much smaller activation volume. The last of the three explanations is that an asthenospheric layer does not exist beneath stable continents. We regard this as the most likely of the three options at this stage, although more work needs to be done. If true, it implies that continents are strongly coupled to general mantle circulation. This conclusion is supported, in the case of the South American plate, by the evidence for a fossil plume beneath Brazil (VANDECAR *et al*., 1995) that appears to have moved with the continent. It appears that the unique structure of stable continents, particularly their stable roots, serve to suppress the development of a mechanical asthensphere (JORDAN, 1978). .This coupling has implications for the forces that ultimately drive the plates and drive orogeny (RUSSO and SILVER, 1996), the interactions between the plates themselves mediated by mantle circulation (SILVER *et al.*, 1998), and finally the possibility that upwelling from the core-mantle boundary can have a significant effect on the motions of the plates (LITHGOW-BERTELLONI and SILVER, 1998).

The orogeny paradox: where does the heat come from?

The second important implication of vertically coherent deformation is that it leads to the orogeny paradox (SILVER and CHAN, 1991; SILVER, 1996; KINCAID and SILVER, 1996), namely that the deformational and thermal properties of many orogenies are apparently inconsistent with the simplest models of mountain building as the collision between plates. On the one hand, the idea of vertically coherent deformation simply requires that plates deform as a whole, and that the chemical distinction between the crust and mantle is of secondary importance. The shortening that is the most direct result of a continental collision should also lead to thickening of the plate. The thickened plate will then have distinct mechanical and thermal properties, namely, a doubly thickened crust and a higher-velocity mantle as geotherms are advected downward. This process has been invoked, for example, to account for the deep roots of Archean cratons (JORDAN, 1978).

This model, however, does not easily explain some of the basic thermal characteristics of orogenies. It predicts that orogenies should be cooling events while it appears that they are often heating events. Perhaps the clearest modern example of this paradox is northern Tibet. The deformed plateau extends some 1000 km north of the suture, so that the northern part of the plateau has most probably not been subjected to subduction-related processes. Yet, northern Tibet is characterized by pervasive surface volcanism, including basaltic volcanism, implying that the lower crust and uppermost mantle are melting. There is also seismological evidence for a hot upper mantle (see SILVER, 1996 and references therein). At the same time, there is excellent evidence for vertically coherent deformation, as noted above. This correspondence between crustal and mantle deformation places a strong constraint on mechanical models. In particular, it is difficult to reconcile this result with convective removal models, where the thickened lithosphere becomes convectively unstable and is replaced by warm asthenosphere (HOUSEMAN *et al*., 1981; MOLNAR *et al*., 1993; CONRAD and MOLNAR, 1999). It should be further noted that the basaltic magmas appear to be derived from a lithospheric, rather than asthenospheric, source (MOLNAR *et al*., 1993), also consistent with the idea that the lithosphere is intact.

One way of explaining the heat without removal of the mantle lithosphere is radioactive heat production. However, this model will not create enough heat in short enough time if the heat-producing elements are concentrated in the upper crust, as is usually assumed. In addition, this process does not account for a hot upper mantle (see KINCAID and SILVER, 1996).

An alternative source of heat that satisfies both the shear wave splitting data and the thermal properties of the mantle, is that the deformation itself is the source of heat (SILVER and CHAN, 1991;

SILVER, 1996; KINCAID and SILVER, 1996). It has been proposed that the strain energy of the deformation is dissipated as heat, and that this heat is sufficient to account for the elevated temperatures inferred for both the crust and the mantle. In order for this to be a significant process, the orogenic stresses have to be high, several kilobars. The largest thermal anomaly will be concentrated where the plate is the strongest, at the very top of the mantle. This strain energy will be very effective in generating lower crustal melts and may also be capable of melting some of the mantle itself, especially if there are volatiles that serve to significantly lower the melting temperature of peridotites. Numerical modeling of this process (KINCAID and SILVER, 1996) predicts a thermal profile that possesses anomalously high temperatures just below the Moho but with anomalously low temperatures at greater depth as would be expected from the advective thickening of the Eurasian plate. Recent tomography from this region (GRIOT *et al.*, 1998), reveals a seismic structure very similar to what would be predicted from viscous heating.

If viscous dissipation indeed plays a role in determining the thermal characteristics of the mantle today, it probably played a more significant role in the Archean. Higher geotherms would have brought deformed mantle material closer to melting (KINCAID and SILVER, 1996), so that viscous dissipation could have been a significant heat source for crust formation. The manner in which early Archean crust formed is still highly controversial, especially the issue of whether or not a plate-tectonic process was involved. Could viscous dissipation, operating on a pervasively deformed oceanic plate, be a viable way to make the first continents? We think this hypothesis is worthy of serious consideration.

Acknowledgments--We take great pleasure in dedicating this article to F. R. "Joe" Boyd who has opened the field of subcontinental mantle geology to the world. We thank Joe for the time he has generously spent with us discussing his ideas about the Archean mantle, and for allowing us to analyze his unique collection of mantle nodules. We also thank Peter Nixon for providing his valuable samples as well. We thank Françoise Boudier and Adolphe Nicolas for their continued encouragement to make a more quantitative approach to upper mantle LPO development and seismic anisotropy. Finally, we acknowledge the effort of the Kaapvaal Craton Project and the menbers of the Kaapvaal Seismic Working Group for making the southern African seismic experiment possible. This work was supported by the Carnegie Institution of Washington. University of Montpellier II and NSF grant # EAR - 9526840.

REFERENCES

ABRAMSON E. H., BROWN J. M., SLUTSKY L. J., and ZANG J. (1997) The elastic constants of San Carlos olivine to 17 GPa. *J. Geophys. Res.* **102**, 12253-12263.

AVÉ-LALLEMANT H. G. (1975) Mechanisms of preferred orientations of olivine in tectonite peridotite. *Geology* **3**, 653-656.

BARRUOL G., SILVER P. G., and VAUCHEZ A. (1997) Seismic anisotropy in the Eastern United States; deep structure of a complex continental plate. *J. Geophys. Res.* **102**, 8329-8348.

BASS J. D., LIEBERMANN R. C., WEIDNER D. J., and FINCH S. J. (1981) Elastic properties from acoustic and volume compression experiments. *Phys. Earth Planet. Inter.* **25**, 140-158.

BASS J. D. (1995) Elasticity of minerals, glasses and melts. In *Minerals Physics and Crystallography: a Handbook of Physical Constants* (ed. T. J. AHRENS), pp. 45-63, American Geophysical Union.

BEN ISMAÏL W. and MAINPRICE D. (1998) An olivine fabric database: an overview of upper mantle fabrics and seismic anisotropy. *Tectonophysics* **296**, 145-157.

BEN ISMAÏL W. and MAINPRICE D. (1999) An orthopyroxene fabric database: implications for seismic anisotropy. *Tectonophysics* **submitted**.

BLACKMAN D. K., KENDALL J.-M., DAWSON P. R., WENK H.-R., BOYCE D., and PHIPPS-MORGAN J. (1996) Teleseismic imaging of subaxial flow at mid-ocean ridges: travel-time effects of anisotropic mineral texture in the mantle. *Geophys. J. Int.* **127**, 415-426.

BLACKMAN D. K. and KENDALL J.-M. (1997) Sensitivity of teleseismic body waves to mineral texture and melt in the mantle beneath a mid-ocean ridge. *Phil. Trans. R. Soc. Lond. A* **355**, 217-231.

BORMANN P., BURGHARDT P. T., MAKEYEVA L. I., and VINNIK L. P. (1993) Teleseismic shear-wave splitting and deformations in Central Europe. In *Dynamics of the Subcontinental Mantle; from Seismic Anisotropy to Mountain Building.*, Vol. 78 (ed. D. MAINPRICE, A. VAUCHEZ, and J. P. MONTAGNER), pp. 157-166. Elsevier.

BORMANN P., GRUENTHAL G., KIND R., and MONTAG H. (1996) Upper mantle anisotropy beneath Central Europe from SKS wave splitting; effects of absolute plate motion and lithosphere-asthenosphere boundary topography? *J. Geodynamics* **22**, 11-32.

BOYD F. R. and ENGLAND J. L. (1960) Apparatus for phase equilibrium measurements at pressures up to 50 kilobars and temperatures up to 1750°C. *J. Geophys. Res.* **65**, 741-748.

BOYD F. R. (1973) A pyroxene geotherm. *Geochim. Cosmochem. Acta* **37**, 2533-2533.

BUTTLES J. and OLSON P. (1998) A laboratory model of subduction zone anisotropy. *Earth Planet. Sci. Lett.* **164**, 245-262.

CARLSON R. W., GROVE T. L., DEWIT M. J., and GURNEY J. J. (1996) Program to study crust and mantle of the Archean Craton in Southern Africa. *Eos, Transactions, American Geophysical Union* **77**, 273.

CHAI M., BROWN J. M., and SLUTSKY L. J. (1997) The elastic constants of an aluminous orthopyroxene to 12.5 GPa. *J. Geophys. Res.* **102**, 14779-14785.

CHASTEL Y. B., DAWSON P. R., WENK H.-R., and BENNET K. (1993) Anisotropic convection with implications for the upper mantle. *J. Geophys. Res.* **98**, 17757-17771.

COLLINS M. D. and BROWN J. M. (1998) Elasticity of an upper mantle clinopyroxene. *Phys. Chem. Minerals* **26**, 7-13.

CONRAD C. and MOLNAR P. (1999) Convective instability of a boundary layer with temperature and strain rate dependent viscosity in terms of "available buoyancy". *Geophys. J. Int.* **submitted**.

DAVIS P., ENGLAND P., and HOUSEMAN G. (1997) Comparison of shear wave splitting and finite strain from the India-Asia collision zone. *J. Geophys. Res.* **102**, 27511-27522.

DEWIT M. J., ROERING C., HART R. J., ARMSTRONG R., RONDE C., GREEN R., TREDOUX M., PEBERDY E., and HART R. A. (1992) Formation of an Archean continent. *Nature* **357**, 553-562.

DUFFY T. S. and VAUGHAN M. T. (1988) Elasticity and its relationship to crystal structure. *J. Geophys. Res.* **93**,

383-391.
ESTEY L. H. and DOUGLAS B. J. (1986) Upper mantle anisotropy: A preliminary model. *J. Geophys. Res.* **91**, 11393-11406.
ETCHECOPAR A. (1977) A plane kinematic model of progressive deformation in a polycrystalline aggregate. *Tectonophysics* **39**, 121-139.
ETCHECOPAR A. and VASSEUR G. (1987) A 3-D kinematic model of fabric development in polycrystalline aggregates: comparison with experimental and natural examples. *J. Struct. Geol.* **9**, 705-717.
FOUCH M. J., FISCHER K. M., PARMENTIER E. M., WYSESSION M. W., and CLARKE T. J. (1999) Shear wave splitting, continental keels and patterns of mantle flow. *J. Geophys. Res.* **submitted**.
FRISILLO A. L. and BARSCH G. R. (1972) Measurement of single-crystal elastic constants of bronzite as a function of pressure and temperature. *J. Geophys. Res.* **77**, 6360-6384.
GAO S. S., SILVER P. G., JAMES D. E., and GROUP K. S. (1998) Seismic structure and tectonics of southern Africa-progress report. *EOS Trans. Am. Geophys. Un.* **79**, 574.
GRIOT D. A., MONTAGNER J. P., and TAPPONNIER P. (1998) Phase velocity structure from Rayleigh and Love waves in Tibet and its neighboring regions. *J. Geophys. Res.* **103**, 21215- 21232.
GRIPP A. E. and GORDON R. G. (1990) Current plate velocities relative to the hotspots incorporating the Nuvel-1 global plate motion model. *Geophys. Res. Lett.* **17**, 1109-1112.
HOUSEMAN G. A., MCKENZIE D. P., and MOLNAR P. (1981) Convective instability of a thickened boundary layer and its relevance for the thermal evolution of continental convergent belts. *J. Geophys. Res.* **86**, 6115-6132.
HUMPHREYS F. J. and HATHERLY M. (1995) *Recrystallization and Related Annealing Phenomena*. Pergamon.
ISSAK D. G. (1992) High-temperature elasticity of iron-bearing olivine. *J. Geophys. Res.* **97**, 1871-1885.
ITA J. and STRIXRUDE L. (1992) Petrology, elasticity and composition of the mantle transition zone. *J. Geophys. Res.* **97**, 6849-6866.
JORDAN T. H. (1978) Composition and development of the continental tectosphere. *Nature* **274**, 544-548.
KANESHIMA S. and SILVER P. G. (1995) Anisotropic Loci in the mantle beneath central Peru. *Phys. Earth Planet. Inter.* **88**, 257-272.
KARATO S. (1992) On the Lehmann Discontinuity. *Geophys. Res. Lett.* **19**, 2255-2258.
KARATO S. (1993) Dislocation recovery in olivine under deep upper mantle conditions: implications for creep and diffusion. *J. Geophys. Res.* **98**, 9761-9768.
KENDALL J. M. and SILVER P. G. (1996) Constraints from seismic anisotropy on the nature of the lowermost mantle. *Nature* **381**, 409-412.
KENDALL J. M. and SILVER P. G. (1998) Investigating causes of D" anisotropy. In *The Core-Mantle Boundary Region*, Vol. Geodynamics **28** (eds. M. GURNIS, M. WYSESSION, E. KNITTLE, and B. BUFFET), pp. 409-412. American Geophysical Union.
KINCAID C. and SILVER P. G. (1996) The role of viscous dissipation in the orogenic process. *Earth Planet. Sci. Lett.* **142**, 271-288.
LEVIEN L., WEIDNER D. J., and PREWITT C. T. (1979) Elasticity of diopside. *Phys. Chem. Minerals* **4**, 105-113.
LITHGOW-BERTELLONI C., and SILVER P. G. (1998) Dynamic topography, plate driving forces and the African superswell. *Nature* **395**, 269-272.
MAINPRICE D. and SILVER P. G. (1993) Interpretation of SKS waves using samples from the subcontinental lithosphere. *Phys. Earth Planet. Inter.* **78**, 257-80.
MATSUI M. and BUSING W. R. (1984) Calculation of the elastic constants and high-pressure properties of diopside, $CaMgSi_2O_6$. *Amer. Mineral.* **69**, 1090-1095.
MCNAMARA D. E., OWENS T. J., SILVER P. G., and WU F. T. (1994) Shear wave anisotropy beneath the Tibetan Plateau. *J. Geophys. Res.* **99**, 13655-13665.
MEADE C., SILVER P. G., and KANESHIMA S. (1995) Laboratory and seismological observations of lower mantle isotropy. *Geophys. Res. Lett.* **22**, 1293-1296.
MINSTER J. B. and JORDAN T. H. (1978) Present-day plate motions. *J. Geophys. Res.* **85**, 5331-5354.
MOLNAR P., ENGLAND P., and MARTINOD J. (1993) Mantle dynamics, uplift of the Tibetan Plateau, and the Indian monsoon. *Rev. Geophys.* **31**, 357-396.
NICOLAS A., BOUDIER F., and BOULLIER A. M. (1973) Mechanism of flow in naturally and experimentally deformed peridotites. *Amer. J. Sci.* **273**, 853-876.
NICOLAS A. (1989) *Structures of Ophiolites and Dynamics of Oceanic Lithosphere*. Kluwer Academic Publishers.
RIBE N. M. (1989) A continuum theory for lattice preferred orientations. *Geophys. J.* **97**, 199-207.
RIBE N. M. and YU Y. (1991) A theory for plastic deformation and textural evolution of olivine polycrystals. *J. Geophys. Res.* **96**, 8325-8335.
RINGWOOD A. E. (1991) Phase transitions and their bearing on the constitution and dynamics of the mantle. *Geochim. Cosmochim. Acta* **55**, 2083-2110.
RUMPKER G. and SILVER P. G. (1998) Apparent shear-wave splitting parameters in the presence of vertically-varying anisotropy. *Geophys J. Int.* **135**, 790-800.
RUSSO R. and SILVER P. G. (1996) Cordillera orogenesis, mantle dynamics, and the Wilson Cycle. *Geology* **24**, 511-514.
SALTZER R., JORDAN T. H., GAHERTY J. B., ZHAO L., and GROUP K. W. (1998) Anisotropic structure of the Kaapvaal craton from surface wave analysis. *EOS Trans. Amer. Geophys. Union* **79**, 574.
SAVAGE M. K. (1999) Seismic anisotropy and mantle deformation: what have we learned from shear wave splitting? *Rev. Geophys.* **37**, 65-106.
SILVER P. G. and CHAN W. W. (1988) Implications for continental structure and evolution from seismic anisotropy. *Nature* **335**, 34-39.
SILVER P. G. and CHAN W. W. (1991) Shear-wave splitting and subcontinental mantle deformation. *J. Geophys. Res.* **96**, 16429-16454.
SILVER P. G. and KANESHIMA S. (1993) Constraints on mantle anisotropy beneath Precambrian North America from a transportable teleseismic experiment. *Geophys. Res. Lett.* **20**, 1127-1130.
SILVER P. G. (1996) Seismic anisotropy beneath the continents: Probing the depths of geology. *Ann. Rev. Earth Planet. Sci.* **24**, 385-432.
SILVER P. G., RUSSO R. M., and LITHGOW-BERTELLONI C. (1998) The coupling of plate motion and plate deformation. *Science* **279**, 60-63.
TAKESHITA T. (1989) Plastic anisotropy in textured mineral aggregates: theories and geological implications. In *Rheology of Solids and of the Earth* (eds. S. KARATO and M. TORIUMI), pp. 237-283. Oxford University Press.
TAKESHITA T., WENK H.-R., MOLINARI A., and CANOVA G. (1990) Simulation of dislocation-assisted plastic flow in olivine polycrystals. In *Deformation Processes in Minerals, Ceramics, and Rocks* (eds. J. D. BARBER and P. G. MEREDITH), pp. 365-377. Hyman Ltd.
TAYLOR G. I. (1938) Plastic strain in metals. *J. Inst. Metals* **62**, 301-324.
TOMMASI A., VAUCHEZ A., and RUSSO R. M. (1996) Seismic anisotropy in ocean basins; resistive drag of the sublithospheric mantle? *Geophys. Res. Lett.* **23**, 2991-2994.
TOMMASI A. (1998) Forward modeling of the development of seismic anisotropy in the upper mantle. *Earth Planet. Sci. Lett.* **160**, 1-13.
TOMMASI A., MAINPRICE D., CANOVA G., and CHASTEL Y. (1999) Viscoplastic self-consistent and equilibrium-based

modeling of olivine lattice preferred orientations. 1.Implications for the upper mantle seismic anisotropy. *J. Geophys. Res.* **submitted**.

VANDECAR J. C., JAMES D. E., and ASSUMPCAO M. (1995) Seismic evidence for a fossil mantle plume beneath South America and implications for plate driving forces. *Nature* **378**, 25-31.

VAUCHEZ A. and NICOLAS A. (1991) Mountain building: strike-parallel motion and mantle anisotropy. *Tectonophysics* **186**, 183-201.

VINNIK L. P., KRISHNA V. G., KIND R., BORMANN P., and STAMMLER K. (1994) Shear wave splitting in the records of the German Regional Seismic Network. *Geophys. Res. Lett.* **21**, 457-460.

WEBB S. L. (1989) The elasticity of the upper mantle orthosilicates olivine and garnet to 3 GPa. *Phys. Chem. Minerals* **16**, 684-692.

WEBB S. L. and JACKSON I. (1993) The pressure dependence of the elastic moduli of single-crystal orthopyroxene $(Mg_{0.8}Fe_{0.2})SiO_3$. *European J. Mineral.* **5**, 1111-1119.

WEIDNER D. J., WANG H., and ITO J. (1978) Elasticity of orthoenstatite. *Phys. Earth Planet. Inter.* **17**, 7-13.

WENK H.-R., BENNET K., CANOVA G. R., and MOLINARI A. (1991) Modelling plastic deformation of peridotite with the self-consistent theory. *J. Geophys. Res.* **96**, 8337-8349.

WENK H.-R., CANOVA G. R., BRECHET Y., and FLANDIN L. (1997) A deformation-based model for recrystallization of anisotropic materials. *Acta Metall. Mat.* **45**, 3283-3296.

WOLFE C. J. and SOLOMON S. C. (1998) Shear-wave splitting and implications for mantle flow beneath the MELT region of the East Pacific Rise. *Science* **280**, 1230-1232.

ZHANG S. and KARATO S. (1995) Lattice preferred orientation of olivine aggregates in simple shear. *Nature* **375**, 774-777.